Contrib Mineral Petrol (2002) 142: 564–581
DOI 10.1007/s00410-001-0311-z

K. Johnson · C.G. Barnes · J.M. Browning
H.R. Karlsson

Petrology of iron-rich magmatic segregations associated with strongly peraluminous trondhjemite in the Cornucopia stock, northeastern Oregon

Received: 30 October 2000 / Accepted: 28 August 2001 / Published online: 14 November 2001

Abstract The Middle Cretaceous Cornucopia stock in the Blue Mountains of northeastern Oregon is a small composite intrusion consisting of hornblende biotite tonalite, biotite trondhjemite, and three cordierite two mica trondhjemite units. Unusual magnetite + biotite-rich tonalitic rocks are associated with the Crater Lake cordierite trondhjemite, the youngest of the intrusions. Oxide-rich tonalites are characterized by high Fe (~47–68 wt% total Fe as FeO), low SiO_2 (< 36 wt%), and enrichments in HFSE and REE ($La_{(N)} = 361–903$). Oxide-rich tonalites appear in a variety of forms, including composite dikes and sheets, in which they are associated with leucocratic tonalite. Leucotonalite is lower in SiO_2 (60–72 wt%) than Crater Lake trondhjemite, and generally has ΣREE contents and Eu anomalies intermediate between the oxide-rich tonalite and Crater Lake compositions. Oxide-rich tonalites crosscut, and are crosscut by, shear zones in the host trondhjemite, indicating their emplacement late in the pluton's crystallization history. Granitic dikes crosscut the composite dikes in all localities. Geochemical considerations and sedimentary-like structures, such as load casts and bedding of magnetite-rich assemblages in the composite dikes and sheets, are suggestive of crystal settling from an Fe-rich parental magma. The Fe-rich liquid parental to the oxide-rich tonalite–leucotonalite pairs formed by extensive, in-situ, plagioclase + quartz-dominated crystallization of strongly peraluminous trondhjemite. Early magnetite saturation in the trondhjemite was suppressed, either because the parental trondhjemitic magma had a lower initial total Fe content or because it had a lower ferric–ferrous ratio, possibly reflecting a lower oxygen fugacity. Accumulation of magnetite from Fe-rich residual magma is a viable mechanism for the concentration of iron, and the subsequent formation of Fe-rich rocks, in calcic siliceous intrusions. Apparently, Fe-enrichment can occur locally in calcic magmas, and is not restricted to rocks of mafic tholeiitic or anorthositic affinity.

K. Johnson (✉) · C.G. Barnes · J.M. Browning · H.R. Karlsson
Department of Geosciences, Texas Tech University,
Box 41053, Lubbock, TX 79409-1053, USA
E-mail: kennjohn@ttacs.ttu.edu
Tel.: +1-806-7423102
Fax: +1-806-7420100

Editorial responsibility: T.L. Grove

Introduction

Rocks rich in iron oxide phases are enigmatic, albeit volumetrically minor, components of many igneous suites, both volcanic and plutonic. Most occurrences are so-called nelsonites (ilmenite + apatite rocks), oxide-apatite gabbronorites (OAGNs), and Kiruna-type deposits associated with Proterozoic anorthosite massifs, alkaline syenitic complexes, and Fe-rich tholeiitic rocks (Ashwal 1982; Kolker 1982; Owens and Dymek 1992; McLelland et al. 1994; Scoates et al. 1996; Ripley et al. 1998, and many others). However, magnetite-rich rocks are also associated with rocks of calc-alkaline affinity (Badham and Morton 1976; Hildebrande 1986; Reid et al. 1993), and include the enormous iron deposits of Kiruna, Sweden (Frietsch 1978) and the magnetite lava flows and volcanic plugs of the Chilean Andes (Grez et al. 1991; Nyström and Henríquez 1994). Despite their subordinate volumes, oxide-rich rocks are important because they provide information about the crystallization histories of the associated magmas.

The objectives most central to the study of such unusual rocks are to establish the source of iron and the mechanism by which it is concentrated. This is currently the subject of much debate. Oxide-rich rocks have been explained by igneous or igneous-related (i.e., hydrothermal) processes as: (1) alteration- and/or replacement-associated deposits from hydrothermal fluids (Hildebrand 1986; Gow et al. 1994; Arancibia and Clark 1996; Barton and Johnson 1996); (2) the Fe-rich end member resulting from liquid immiscibility (Philpotts

1967, 1982; Badham and Morton 1976; Kolker 1982; Ripley et al. 1998), where, in some instances, liquid immiscibility may have been triggered by assimilation of Fe-rich wall rocks (Lundberg and Smellie 1979); (3) cumulates from an evolving magma (Wager and Brown 1968; Reid et al. 1993); and (4) residual Fe-rich liquid resulting from fractional crystallization (Bateman 1951; McLelland et al. 1994; Vander Auwera et al. 1998), where the concentration of iron may be accomplished by deformation (Duchesne 1999), or magnetite accumulation (Scoates et al. 1996).

The Middle Cretaceous Cornucopia stock in the Blue Mountains of northeastern Oregon consists of several distinct units of calcic high-alumina tonalite and trondhjemite, some of which are cordierite-bearing. Oxide (magnetite)-rich tonalitic rocks (hereafter referred to as ORTs) occur in a variety of forms in close association with the youngest intrusive unit. This occurrence is particularly noteworthy because magnetite-rich rocks have not previously been described associated with strongly peraluminous trondhjemites. In this paper, we describe the petrology and geochemistry of ORTs in the Cornucopia stock, demonstrate a genetic relationship between the ORTs and host trondhjemite, and discuss various mechanisms by which the ORTs could have formed. We present evidence that suggest the ORTs are cumulates from a local Fe-enriched residual liquid produced by crystallization at the margins of their host trondhjemite. This interpretation may have implications for the formation of similar oxide-rich accumulations in calc-alkaline plutons (Badham and Morton 1976; Reid et al. 1993).

Geologic setting

The Blue Mountains province is a complex assemblage of at least four oceanic and island arc terranes that were amalgamated and accreted as a package to the North American continental margin during Late Jurassic to Middle Cretaceous time. At the terrane/continent suture, metamorphism associated with accretion reached a peak at $\sim 128 \pm 3$ Ma (Getty et al. 1993). Late Jurassic to Middle Cretaceous magmatism in the Blue Mountains occurred in two pulses (Johnson 1995). The first pulse ($\sim$158–137 Ma; ''pre-accretion'') is manifest as large, composite plutons ranging in composition from gabbro to granite. They were emplaced shortly before and during the earliest stages of terrane accretion. Their compositions are generally consistent with interaction of mantle and crustal sources (Johnson 1995). The second pulse ($\sim$125–117 Ma; ''post-accretion'') resulted in the intrusion of small, relatively homogeneous tonalitic and trondhjemitic plutons that were generated by crustal melting in response to the accretion event (Johnson et al. 1997).

The Cornucopia stock represents a distinctive subset of the post-accretion plutons. It is unusual because its high-alumina compositions allowed for the crystallization of cordierite. The stock is composite and consists of five distinct intrusive units. They include, in order of intrusion, the Cornucopia hornblende biotite tonalite, Tramway biotite trondhjemite, Big Kettle cordierite two mica trondhjemite, Pine Lakes cordierite two mica trondhjemite, and the Crater Lake cordierite two mica trondhjemite (Fig. 1; Taubeneck 1964). The stock was emplaced in a short time interval, as shown by identical concordant biotite $^{40}Ar/^{39}Ar$ ages of 116.8 ± 1.2 Ma for the Cornucopia tonalite and the Crater Lake trondhjemite (Johnson et al. 1997). Dikes of biotite ($\pm$ hornblende) dacite and biotite granodiorite occur only in the older Cornucopia and Tramway units, whereas dikes of cordierite two mica granite are restricted to the Pines Lakes and Crater Lake units. Intrusive breccias and cm-scale quartz veins are interspersed throughout the pluton, and suggest the Cornucopia magmas were H_2O-rich.

The Cornucopia tonalitic and trondhjemitic magmas were generated by deep-seated partial melting of low-K metabasaltic rocks of the host Wallowa terrane (Johnson et al. 1997). These magmas were in equilibrium with an amphibole + clinopyroxene + garnet residual assemblage, which suggests a pressure of melting of $\geq$10 kbar and temperatures exceeding 900 °C (e.g., Wolf and Wyllie 1993, 1994). The magmas were emplaced at upper crustal levels equivalent to pressures slightly less than 2 kbar, under fairly oxidizing conditions loosely constrained between the FMQ and HM buffers (Johnson 1995; Johnson et al. 1997).

Summary of lithologies

Oxide-rich tonalites within the Cornucopia stock are most common in the Crater Lake trondhjemite, especially near its southern intra-plutonic contact with the Cornucopia tonalite (Fig. 1). Oxide-rich tonalites crosscut, and are crosscut by, shear zones within the host trondhjemite (Fig. 2a), indicating their emplacement late in the pluton's history. Late-stage granitic dikes crosscut the ORTs in all localities (Fig. 2b).

Crater Lake trondhjemite

Cordierite-bearing trondhjemites of the Crater Lake unit contain coarse-grained assemblages of plagioclase + quartz + biotite + muscovite + cordierite + magnetite $\pm$ K-feldspar. Some samples are porphyritic, with phenocrysts of plagioclase, quartz, biotite, and cordierite. K-feldspar is interstitial. Accessory minerals are apatite, sphene, and zircon.

Blue-green cordierite occurs as large euhedral to subhedral columnar crystals that are typically pinitized. Unaltered cordierite is unzoned, is magnesium-rich with $Mg/(Mg + Fe_{tot})$ values of 0.73–0.77 (Johnson et al. 1997), and is considered to be magmatic rather than xenocrystic (Taubeneck 1964, 1987; Johnson et al. 1997).

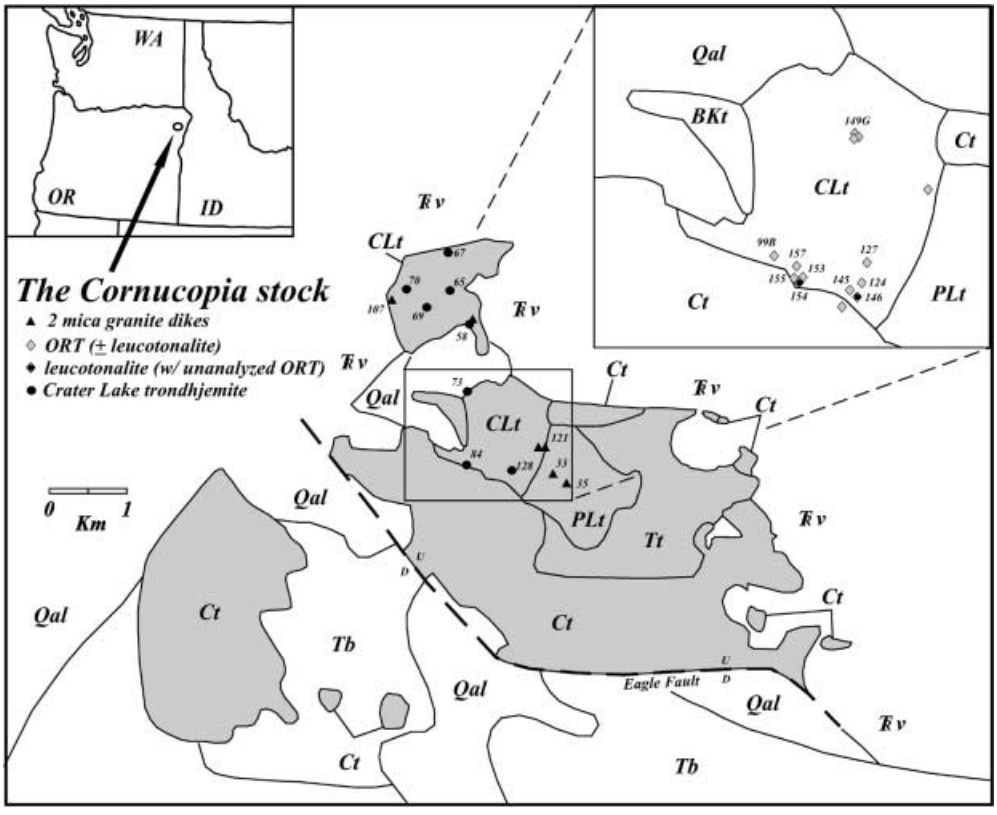

Fig. 1 Generalized map of the Crater Lake unit of the Cornucopia stock, showing sample localities. Modified from Taubeneck (1964). *Ct* Cornucopia tonalite; *Tt* Tramway trondhjemite; *BKt* Big Kettle trondhjemite; *PLt* Pine Lakes trondhjemite; *CLt* Crater Lake trondhjemite; *TRv* undifferentiated greenschist facies mafic volcanic and volcaniclastic rocks; *Tb* flood basalts of Miocene age; *Qal* alluvium. *Unlabeled symbols* are unanalyzed samples

Intraplutonic contacts of the Crater Lake unit are generally sharp and characterized by magmatic brecciation, quartz veins, wall rock xenoliths, schlieren, pegmatitic to aplitic dikes, and mylonitic shear zones. Some dikes of Crater Lake trondhjemite emplaced into the surrounding country rocks are coarse-grained and lack chilled margins, whereas others are porphyritic with phenocrysts of plagioclase, quartz, and cordierite in a groundmass of plagioclase + quartz + biotite + magnetite.

Oxide-rich tonalite and leucotonalite

Oxide-rich tonalites in the Cornucopia stock occur as thin, vein-like stringers, isolated lens-shaped pods, and tabular sheets and dikes. In some localities, ORTs are associated with pegmatitic trondhjemite or, more rarely, pegmatitic granite. In one locality, thin dikes (< 10 cm in width) of pegmatitic tonalite with biotite-rich margins terminate as thin veins (< 1 cm wide) of almost pure magnetite. In several localities, veins of magnetite fill fractures in the host trondhjemite.

A number of composite dikes in the area consist of ORT and leucotonalite. These dikes are up to 10 cm thick and are greater than ~100 m in exposed length. The dikes vary in thickness along strike and some bifurcate to form two or more separate, closely spaced dikes. Contacts between these composite dikes and the host trondhjemite are generally sharp (Fig. 2c). A xenolith of the trondhjemitic host was observed in one composite dike, which suggests brittle behavior of the host rocks. Where ORT and leucotonalite are present in subhorizontal composite sheets, the leucotonalite overlies the ORT. In some sheets magnetite-rich ORT grades upward to biotite- and magnetite-poor leucotonalite. Oxide-rich tonalites commonly display structures reminiscent of those in sedimentary rocks, such as load casts, bedding-like layering, and slumping (Fig. 2d, e).

In addition to structures suggesting gravitational settling, some dikes contain small, isolated ORT fragments dispersed in a leucotonalitic host. These fragments are commonly connected to each other by thin stringers of magnetite. In addition, angular clots of pinitized cordierite, several centimeters in longest dimension, are observed in these leucotonalitic dikes. Cordierite within the clots is up to 2 cm in length, and exhibits igneous lamination with minor interstitial quartz and plagioclase.

ORTs consist of exsolved magnetite (with lamellae of ilmenite and titaniferous magnetite) + biotite + plagioclase + quartz + muscovite + apatite ± cordierite ± K-feldspar (Table 1). ORTs exhibit a seriate grain size distribution with hypidiomorphic granular texture. Plagioclase, quartz, and K-feldspar are in approximately tonalitic proportions (Streckeisen 1973), hence the name "oxide-rich tonalite". Magnetite is euhedral to subhedral, ranges from coarse- to medium-grained, and reaches ~66% by volume (Table 1). In some samples, anhedral glomerocrysts of magnetite enclose cordierite,

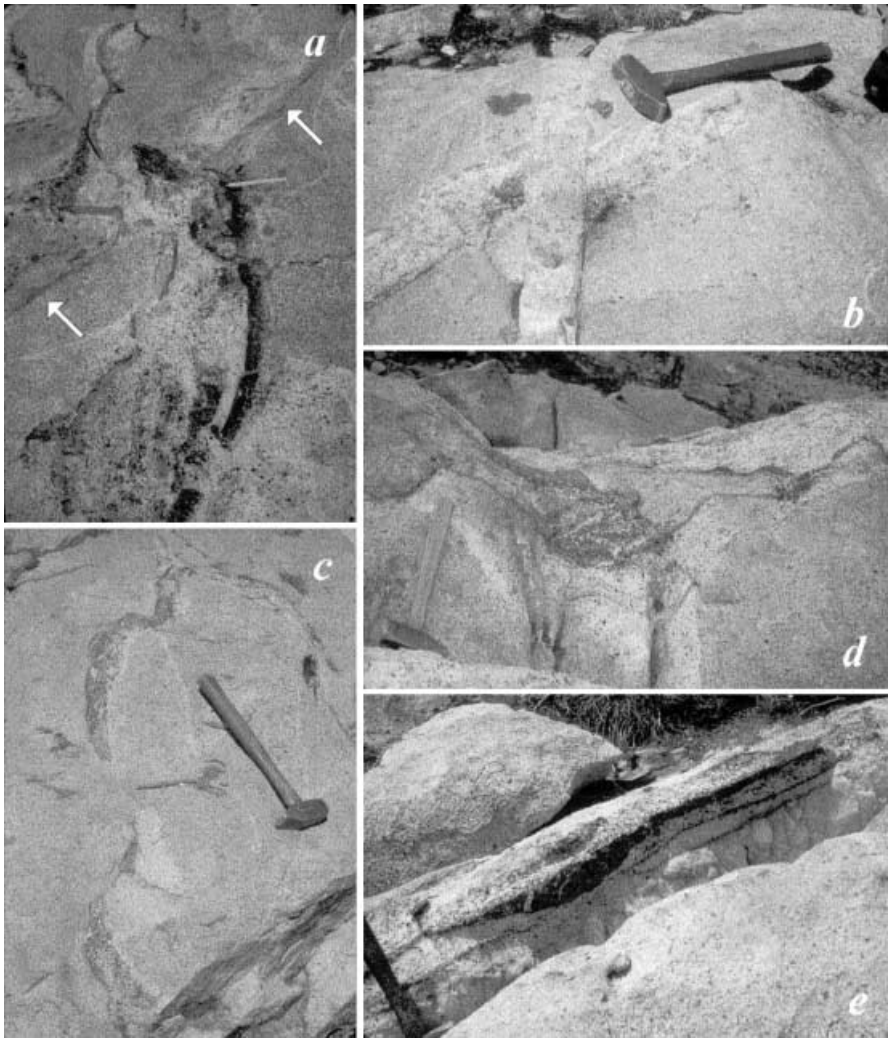

Fig. 2 Photographs of ORT occurrences in the Crater Lake trondhjemite. **a** ORT-bearing composite dike cut by shear zone (designated with *arrows*). *Pen magnet* is approximately 12 cm in length. **b** Magnetite-rich accumulation in composite dike cut by late-stage granitic dike. **c** Asymmetric ORT-bearing composite dike. The dike was pinched closed, leaving behind magnetite-rich clots below the tip of the pen magnet. **d** Magnetite-rich slump feature in an ORT/leucotonalite composite dike. **e** Magnetite-rich accumulation, interpreted as a load cast, in an ORT/leucotonalite composite dike

plagioclase, quartz, and biotite. Quartz is typically interstitial, whereas biotite occurs as large euhedral phenocrysts and as an interstitial phase. Where present, pinitized cordierite occurs in a wide range of sizes (up to approximately 1 cm in length). Large euhedral apatite crystals reach 5% by volume.

Coarse-grained leucotonalite is hypidiomorphic granular and contains plagioclase + quartz + biotite + K-feldspar + oxides + muscovite ± cordierite (Table 1). Tonalite associated with ORT is termed "leucocratic" on the basis of its generally biotite-poor nature, relative to the host Crater Lake trondhjemite. However, "leucotonalite" adjacent to ORT can contain substantial amounts of biotite (up to 13 vol%) and magnetite (up to 2 vol%).

Granitic dikes

Dikes of cordierite two-mica granite are common in the Crater Lake and Pine Lakes trondhjemites. They are generally fine-grained or porphyritic, are typically less than 5 cm thick, and may contain muscovite, biotite, and/or cordierite. Accessory minerals are Fe–Ti oxides (magnetite, Ti-magnetite, and ilmenite), apatite, zircon, and rare garnet and pyrophanite. Plagioclase, quartz, K-feldspar, and cordierite occur as phenocrysts in porphyritic samples. Plagioclase is sodic ($< An_{10}$; Johnson 1995). MnO contents in ilmenite lamellae in magnetite are high (~22–24 wt%; Johnson 1995).

Geochemistry

Analytical methods

Modal compositions of stained thin sections were determined by standard point counting techniques (1,000 points per sample). Biotite compositions were obtained with a Cameca SX-50 electron probe microanalyzer at the Ohio State University (see Johnson et al. 1997).

Oxygen was extracted from quartz, biotite, and whole rock powders using BrF_5 after the method of Clayton and Mayeda (1963). Oxygen was converted to CO_2 by reacting over a hot carbon rod, and CO_2 yields were measured on-line. Only those samples with CO_2 yields of

Table 1 Modal mineralogy of selected samples of Crater Lake trondhjemite, ORTs, leacotonalite, and granite. Cordierite percentages include pinite pseudomorphs (see Johnson et al. 1997). Accessory minerals are zircon and sphene (and apatite in trondhjemitic and granitic samples). Secondary minerals are sericite (and epidote and chlorite in trondhjemitic and granitic samples). *tr* Trace abundances

	Crater Lake trondhjemite					ORTs								Leucotonalites				Granites			
	58	65	67	70	84	99B	124B	149C	147	145B	149G	155B	157	155A	145A	124C	146A	33	107	35	60
Plagioclase	54.2	53.8	49.0	66.3	58.8	20.5	21.6	13.4	9.1	20.1	4.8	20.0	5.1	55.8	67.0	68.9	58.9	36.8	36.0	38.0	30.1
Quartz	36.6	38.6	41.9	27.7	35.0	2.4	12.3	7.3	3.1	16.2	7.2	15.9	10.5	29.6	24.6	16.2	33.1	27.2	31.5	31.4	36.0
K-Feldspar	4.3	3.0	3.9		2.3		4.1			1.9		2.2	0.1	0.3	2.2	3.8	0.7	32.2	25.6	25.8	30.0
Biotite	2.6	2.4	2.9	2.3	1.5	6.8	12.8	8.0	9.7	13.1	15.4	9.6	11.0	12.6	0.2	8.8	0.8				0.2
Fe–Ti oxides	0.4	0.7	0.1	0.2	0.1	59.9	46.1	63.4	64.3	38.9	65.7	47.9	59.8	0.6	0.2	0.7	0.2	0.2		0.1	0.1
Cordierite	0.2	0.7	0.1	0.5	0.6			2.2			2.7	1.2	2.8					tr	2.5	2.6	0.2
Muscovite	1.0	0.1	1.9	2.6	1.5	0.8	2.1	1.1	8.6	8.2	2.2	1.9	6.2	0.3	3.1	1.0	3.9	1.5	4.1	0.9	3.2
Apatite						1.9	0.1	1.1	5.0	0.6	1.1	0.1	3.0	0.1	0.2		0.1				
Chlorite						6.1	0.3	1.8		0.8	0.9	0.1	s1.5	0.6	1.4	0.4	2.1				
Epidote							0.1								0.3						
Accessory minerals	0.2	0.1				0.3	0.2	0.1	0.2	0.1					0.5	0.2	0.2		tr		
Alteration and secondary minerals	0.5	0.3	0.2	0.4	0.2	1.2		1.6		0.1		1.1		0.1	0.3			2.1	0.1	0.7	0.2

$100^{+0.5}/_{-1.0}$% were accepted. Oxygen isotope ratios were determined with a VG Micromass SIRA 12 mass spectrometer at Texas Tech University, and are reported relative to V-SMOW. The cumulative value for NBS-28 determined by this lab is $+9.49 \pm 0.20$‰.

All whole-rock powders were analyzed by ICP-AES at Texas Tech University. Rare earth elements, Co, Sb, Cs, Hf, Ta, Th, and U were analyzed by INAA at Oregon State University on samples prepared in an alumina shatterbox. Rubidium was determined by flame emission spectrometry. ORTs were analyzed using the method of Salisbury et al. (1999). Sample powders were mixed with pure quartz (Hot Springs, Arkansas) and $LiBO_2$ in fixed proportions and fused in graphite crucibles. Molten samples were then quenched and dissolved in dilute HCl. Samples were analyzed repeatedly over a period of several weeks. Only Zr precipitated appreciably from solution during that time. Total Fe was also determined by volumetric titration and INAA. With the exception of one sample (127), differences in total Fe between ICP-AES and volumetric titration were less than 6%, and those between ICP-AES and INAA were less than 9%. Other elements determined by INAA with low reported uncertainties, such as Na_2O (3%), Sc (3%), and Zn (5%), were in agreement with the ICP-AES results (Salisbury et al. 1999).

Major, trace, and rare earth elements

The Cornucopia stock possesses characteristics of a high-alumina tonalite–trondhjemite–granitoid suite (high-Al TTG; Barker 1979; Drummond and Defant 1990), such as >15 wt% Al_2O_3 at the 70 wt% SiO_2 level, >300 ppm Sr, and low Y (<15 ppm). The entire suite spans a range of SiO_2 contents between 65 and 74 wt%. The Crater Lake trondhjemite spans a narrower range of SiO_2 contents, from about 70 to 74 wt% (Fig. 3a; Table 2). The Crater Lake unit has lower total Fe than the other cordierite trondhjemites with similar Al_2O_3 contents (inset of Fig. 3c). Like other units of the Cornucopia stock, rocks of the Crater Lake trondhjemite exhibit steep, nearly linear chondrite-normalized rare earth element (REE) patterns [$(La/Lu)_N = 11.8–12.5$], low heavy REE abundances, and slight positive Eu anomalies ($Eu/Eu^* = 1.03–1.12$; Fig. 4a).

Most cordierite-bearing trondhjemite samples from the Cornucopia stock are mildly peraluminous with respect to the alumina saturation index (A/CNK = 1.0–1.1), despite the presence of cordierite, which is characteristic of strongly peraluminous rocks. For that reason, Johnson et al. (1997) chose the modified alumina saturation index (A*) of Patiño Douce (1992) as a more appropriate measure of alumina activity in the tonalitic and trondhjemitic rocks, where $A^* = (A/CNK) \times$ mol%$(Na_2O + K_2O)$. Johnson et al. (1997) showed that muscovite + cordierite-bearing rocks in the Cornucopia stock have $A^* > 6.40$, which is consistent with the boundary between mildly peraluminous and strongly peraluminous glasses determined by Patiño Douce (1992). Trondhjemitic rocks from the Crater Lake unit have A* values of 6.60–7.14.

Oxide-rich tonalite samples are characterized by high total Fe (47–61 wt% FeO) and low SiO_2 (<36 wt%; Fig. 3). Relative to tonalitic and trondhjemitic rocks of the Cornucopia stock, ORTs are enriched in TiO_2, MnO, P_2O_5, Sc, V, Zn, Zr, Y, Nb, Sb, Ta, Th, U, and Co, and are lower in Al_2O_3, CaO, Na_2O, and Sr (Fig. 3; Table 2). Trends of ORT samples for several elements are orthogonal to the trondhjemitic trends (Fig. 3). A* values for ORT samples range from 1.30 to 5.13. Oxide-rich tonalites are characterized by high ΣREE ($La_N = 361–903$), and exhibit LREE-enriched chondrite-normalized patterns [$(La/Lu)_N \sim 13–39$] with pronounced negative Eu anomalies ($Eu/Eu^* = 0.25–0.32$; Fig. 4b). Zr and Hf in the ORTs show a strong positive

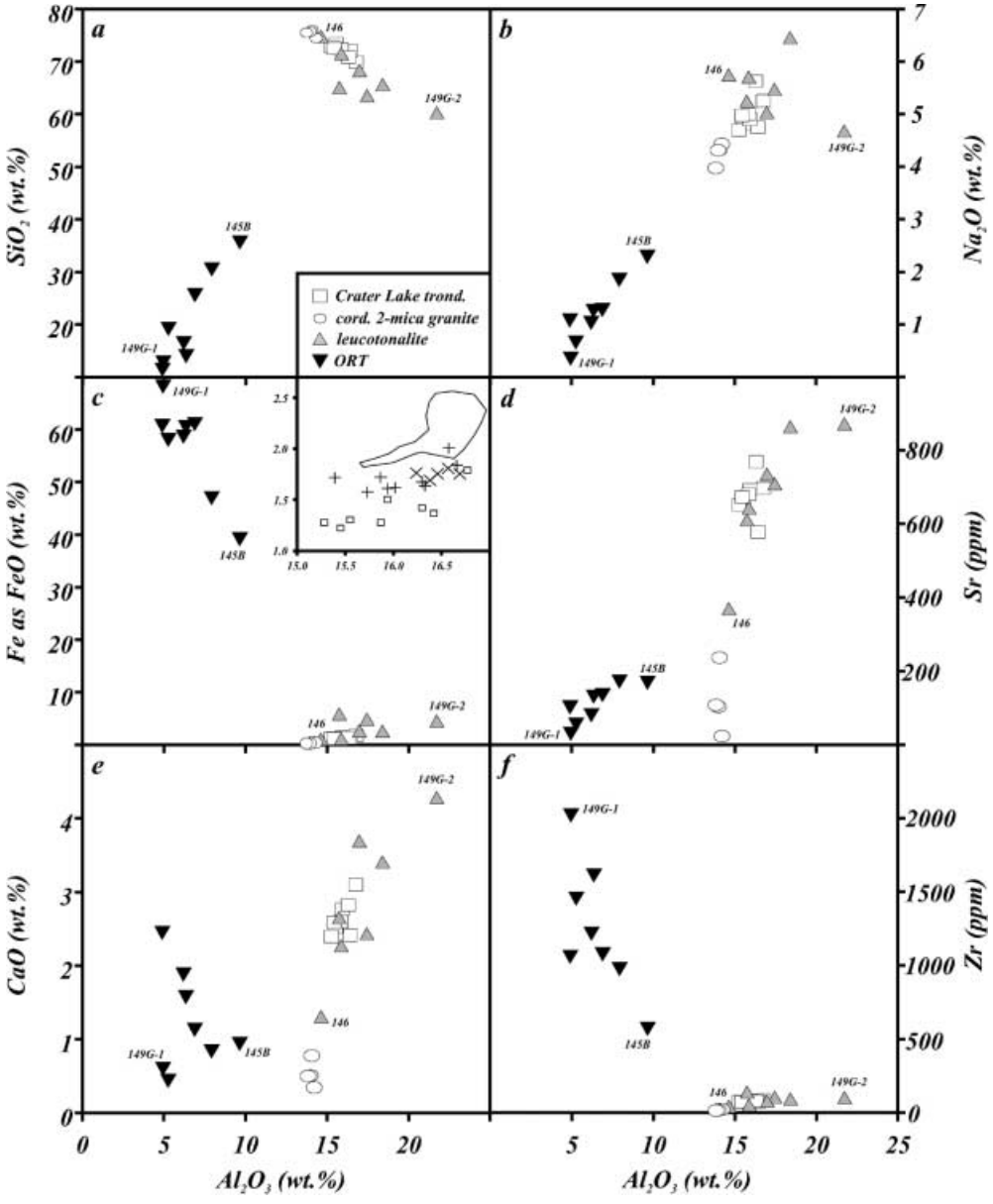

Fig. 3a–f Major and trace element compositions of Crater Lake trondhjemite, leucotonalite, ORT, and granitic dike samples. *Inset* of **c** shows compositional trend of Crater Lake trondhjemite in comparison to those of the Big Kettle (*X*), Pine Lakes (+), and the cordierite-free Tramway and Cornucopia units (*outlined field*)

correlation (not shown), suggesting that zircon is responsible for variations in these elements.

Compared with the Crater Lake trondhjemite, leucotonalite is generally lower in SiO_2 (64–72 wt%; Fig. 3a, Table 2). Sample 146 A (with ~75 wt% SiO_2) is not from a composite dike, but contained small isolated ORT fragments. In general, leucotonalites have higher TiO_2, total Fe, MgO, V, Y, and Co abundances than rocks of the Crater Lake trondhjemite (Table 2). Leucotonalitic rocks have A* values from 6.33 to 8.17. Tonalite is characterized by ΣREE values intermediate to the Crater Lake trondhjemite and ORT and a wide range of Eu/Eu* values (0.52–1.14; Fig. 4c).

One ORT sample with a relatively high proportion of felsic minerals (sample 149G) was hand-separated into melanocratic (149G-1) and leucocratic (149G-2) portions, each containing small (< 1 cm) chips. The chips were then crushed into individual grains and smaller multi-grain clumps, hand-purified (estimated > 90% purity), and analyzed individually. Our purpose was only to determine if the composition of the leucocratic portion of this sample bore any similarities to those of the leucotonalitic samples. The melanocratic portion (predominantly magnetite + biotite) is virtually identical to other ORT samples (Figs. 3 and 4b), but is slightly higher in total Fe (~68 wt% FeO). In comparison to the leucotonalites, sample 149G-2 (predominantly plagioclase + cordierite + quartz) had a greater abundance of cordierite, and is lower in SiO_2, K_2O, Rb, and Ba, and higher in Al_2O_3, CaO, and Sr (Table 2). However, the chondrite-normalized REE pattern for sample 149G-2 is identical to those of the leucotonalites (Fig. 4c).

Granitic rocks in the Crater Lake and Pine Lakes units are characterized by high SiO_2 (> 73 wt%), K_2O,

Table 2 Major and trace element and oxygen isotope compositions of selected samples. *b.d.* Below detection; *n.d,* not determined; *A/CNK* molar ($Al_2O_3/CaO+Na_2O+K_2O$); *A** A/CNK×mol%(Na_2O+K_2O); see text for discussion

	Crater Lake trondhjemite								ORTs								Leucotonalites								Granites			
	58	65	67	70	69	73	84	128	99B	127	155B	149G-1	124	157	153	145B	155A	149G-2	124C	146A	144B	154	145A	33	107	121B	35
SiO_2	69.99	73.48	72.16	72.88	71.98	72.36	72.59	70.92	14.02	25.62	30.52	12.85	19.20	16.48	11.45	35.65	65.14	60.31	63.57	74.82	68.41	65.67	71.58	75.73	74.84	75.58	75.47
TiO	0.19	0.15	0.15	0.15	0.15	0.14	0.16	0.17	3.68	2.47	2.72	3.15	3.67	2.28	2.76	1.83	0.47	0.27	0.52	0.15	0.29	0.22	0.14	0.07	0.06	0.05	0.05
Al_2O_3	16.77	15.55	16.42	15.28	15.94	15.87	15.45	16.30	6.37	6.89	7.92	4.97	5.29	6.22	4.91	9.66	15.76	21.75	17.46	14.65	16.99	18.43	15.90	14.07	14.20	13.98	13.85
FeO	1.79	1.30	1.37	1.28	1.50	1.28	1.22	1.42	60.57	61.13	47.00	68.24	58.07	58.70	60.80	39.20	5.93	4.60	4.91	1.14	2.69	2.67	1.20	0.46	0.42	0.37	0.37
MnO	0.08	0.06	0.07	0.08	0.08	0.07	0.06	0.07	0.93	1.01	0.78	1.31	0.83	1.04	1.05	0.60	0.16	0.25	0.16	0.05	0.09	0.09	0.05	0.04	0.11	0.04	0.03
MgO	0.59	0.50	0.49	0.47	0.48	0.48	0.52	0.52	1.14	0.88	0.78	0.79	0.89	1.05	0.89	1.00	0.91	1.71	1.42	0.42	0.99	0.74	0.46	0.22	0.13	0.17	0.19
CaO	3.10	2.53	2.42	2.40	2.77	2.60	2.59	2.83	1.58	1.13	0.84	0.60	0.44	1.88	2.45	0.94	2.66	4.29	2.44	1.31	3.70	3.41	2.28	0.78	0.35	0.51	0.50
Na_2O	5.26	4.81	4.76	4.70	4.91	5.01	4.98	5.63	1.26	1.28	1.85	0.36	0.66	1.04	1.08	2.29	5.26	4.69	5.48	5.76	5.04	6.46	5.72	4.33	4.44	4.32	3.98
K_2O	1.28	1.13	1.42	1.35	1.07	1.12	1.18	1.06	0.71	1.14	1.02	0.74	1.92	1.01	0.65	1.83	1.18	0.52	2.01	0.99	1.02	0.88	1.55	4.48	4.25	3.99	4.68
P_2O_5	0.10	0.11	0.09	0.11	0.11	0.09	0.10	0.09	0.90	0.61	0.16	0.41	0.24	1.29	1.63	0.26	0.14	0.07	0.12	0.16	0.20	0.07	0.12	0.22	0.33	0.20	0.28
LOI	0.62	0.56	0.77	0.72	0.68	0.84	0.76	0.82	n.d.	n.d.	n.d.	n.d.	n.d.	n.d.	n.d.	n.d.	1.23	1.30	0.98	0.71	0.99	0.67	0.88	0.40	0.66	0.57	0.51
Total	99.76	100.18	100.13	99.40	99.67	99.85	99.61	99.83	91.16	102.16	93.59	93.42	91.21	90.98	87.67	93.27	98.82	99.75	99.07	100.15	100.40	99.31	99.86	100.80	99.79	99.78	99.90
Sc	3.0	2.0	2.4	2.2	2.3	2.2	2.1	2.6	17.0	11.4	16.3	17.7	18.2	15.9	13.7	12.8	4.3	1.8	5.8	1.4	3.0	2.8	2.0	2.0	3.9	2.0	1.6
V	10	13	9	10	14	8	9	10	638	530	440	593	548	660	707	397	50	30	37	9	28	23	9	5	3	3	4
Cr	b.d.	b.d.	5	b.d.	11	26	b.d.	6	43	12	19	11	30	9	44	67	12	5	10	6	10	b.d.	6	17	b.d.	12	b.d.
Cu	b.d.	b.d.	147	5	1	2	b.d.	1	1	5	1	1	b.d.	13	1	9	9	10	7	4	5	13	14	b.d.	3	2	4
Zn	26	26	48	23	41	19	21	29	904	655	638	1,258	420	898	848	382	70	99	68	25	64	35	25	19	11	9	12
Nb	6	4	7	6	7	7	4	9	9	5	19	9	44	2	4	24	6	3	10	2	4	3	4	3	19	11	14
Y	9.1	6.7	7.5	7.0	7.8	6.3	8.2	7.1	79.2	61.3	131.7	216.7	102.7	86.7	101.7	67.3	17.5	14.3	10.7	14.3	11.3	5.1	7.1	4.5	4.9	5.8	3.1
Zr	88	77	75	79	87	70	76	80	1,614	1,078	978	2,021	1,458	1,218	1,061	571	143	106	108	46	so	96	53	25	23	19	17
Ba	679	717	712	723	607	574	720	568	400	478	488	298	474	441	294	741	624	291	942	682	514	597	923	1,210	154	1,842	531
Sr	698	672	579	652	694	681	674	770	131	136	173	31	56	81	102	169	613	874	710	371	736	865	644	238	24	104	109
Rb	15	13	19	17	13	14	15	15	17	20	17	13	27	23	20	27	18	6	31	11	13	14	18	41	67	38	47
Co	n.d.	1.68	n.d.	n.d.	n.d.	n.d.	1.51	n.d.	40.40	26.70	26.10	37.40	22.90	37.90	37.20	19.40	4.93	3.42	5.14	0.89	3.66	2.80	1.50	0.67	n.d.	0.23	n.d.
Sb	n.d.	0.05	n.d.	n.d.	n.d.	n.d.	0.16	n.d.	0.21	0.34	0.18	0.31	0.42	0.28	0.49	0.40	0.26	0.15	0.37	0.22	0.10	0.22	0.29	0.61	n.d.	0.16	n.d.
Cs	n.d.	0.38	n.d.	n.d.	n.d.	n.d.	0.67	n.d.	0.89	0.62	0.56	0.56	1.23	1.02	1.82	1.02	0.92	0.62	1.29	0.48	0.65	0.52	0.49	0.48	n.d.	0.34	n.d.
Hf	n.d.	2.02	n.d.	n.d.	n.d.	n.d.	1.93	n.d.	32.90	24.70	22.30	37.10	29.60	24.80	24.20	16.50	4.17	2.93	3.27	1.65	2.34	2.69	1.95	1.21	n.d.	1.13	n.d.
Ta	n.d.	0.22	n.d.	n.d.	n.d.	n.d.	0.24	n.d.	0.63	0.64	0.89	0.91	2.80	0.42	0.40	1.33	0.30	0.08	0.42	0.26	0.12	0.13	0.24	0.38	n.d.	0.49	ii.d.
Th	n.d.	0.39	n.d.	n.d.	n.d.	n.d.	0.53	n.d.	17.30	9.86	14.20	14.90	19.70	9.43	6.88	7.87	1.82	0.73	1.04	0.37	0.80	1.45	0.46	0.06	n.d.	0.10	n.d.
La	n.d.	9.7	n.d.	n.d.	n.d.	n.d.	11.5	n.d.	290.0	178.0	239.0	252.0	298.0	154.0	119.0	132.0	31.5	15.6	20.7	8.6	12.2	20.5	11.4	2.2	n.d.	2.1	n.d.
Ce	n.d.	19.4	n.d.	n.d.	n.d.	n.d.	21.5	n.d.	613.0	353.0	521.0	572.0	633.0	351.0	282.0	275.0	69.5	36.0	45.6	19.8	26.8	44.3	24.0	3.3	n.d.	5.1	n.d.
Nd	n.d.	8.3	n.d.	n.d.	n.d.	n.d.	10.8	n.d.	282.0	164.0	238.0	277.0	282.0	172.0	154.0	126.0	32.1	18.3	22.2	9.6	13.6	20.5	11.7	1.4	n.d.	3.5	n.d.
Sm	n.d.	1.55	n.d.	n.d.	n.d.	n.d.	1.77	n.d.	44.00	27.10	36.90	47.70	39.60	25.10	25.00	19.30	5.41	3.75	3.26	1.92	2.34	2.79	1.80	0.58	n.d.	0.76	n.d.
Eu	n.d.	0.48	n.d.	n.d.	n.d.	n.d.	0.53	n.d.	3.35	2.08	2.97	3.71	3.01	2.35	2.37	1.62	0.83	0.62	0.62	0.40	0.72	0.80	0.52	0.14	n.d.	0.12	n.d.
Tb	n.d.	0.20	n.d.	n.d.	n.d.	n.d.	0.16	n.d.	3.29	2.45	3.99	5.43	4.53	2.87	3.22	1.96	0.66	0.53	0.32	0.36	0.34	0.21	0.22	0.11	n.d.	0.14	n.d.
Yb	n.d.	0.60	n.d.	n.d.	n.d.	n.d.	0.60	n.d.	5.52	5.05	13.30	18.30	12.70	6.81	6.79	6.05	2.04	1.62	1.04	1.31	1.09	0.54	0.68	0.50	n.d.	0.68	n.d.
Lu	n.d.	0.08	n.d.	n.d.	n.d.	n.d.	0.10	n.d.	0.77	0.76	1.42	1.96	1.33	0.90	0.94	0.72	0.29	0.24	0.13	0.19	0.14	0.08	0.09	0.07	n.d.	0.10	n.d.
Eu/Eu*		1.03					1.12		0.30	0.29	0.28	0.27	0.26	0.32	0.31	0.30	0.52	0.53	0.69	0.61	0.98	1.14	0.97	0.7		0.46	
$\delta^{18}O$ (wr)		8.3					8.2										8.2	7.4	8.3	8.5	8.2	8.3	8.4	9.5	8.6	8.4	9.4
$\delta^{18}O$ (qtz)		9.6									9.2	9.4	9.6	9.7	9.6	9.4	9.3	9.4	9.4	9.6	9.1	9.3	9.3				
$\delta^{18}O$ (bio)											5.0	5.0	4.4	5.1	4.8	4.8											
A/CNK	1.07	1.13	1.19	1.13	1.12	1.12	1.09	1.05	1.11	1.28	1.40	2.01	1.33	1.00	0.71	1.30	1.07	1.35	1.12	1.13	1.05	1.04	1.05	1.05	1.13	1.13	1.11
A*	6.86	6.60	7.14	6.69	6.65	6.79	6.62	7.03	2.26	2.68	3.96	1.92	2.99	2.00	1.30	5.13	6.90	7.34	8.17	7.58	6.33	7.79	7.42	8.00	8.67	8.31	8.24

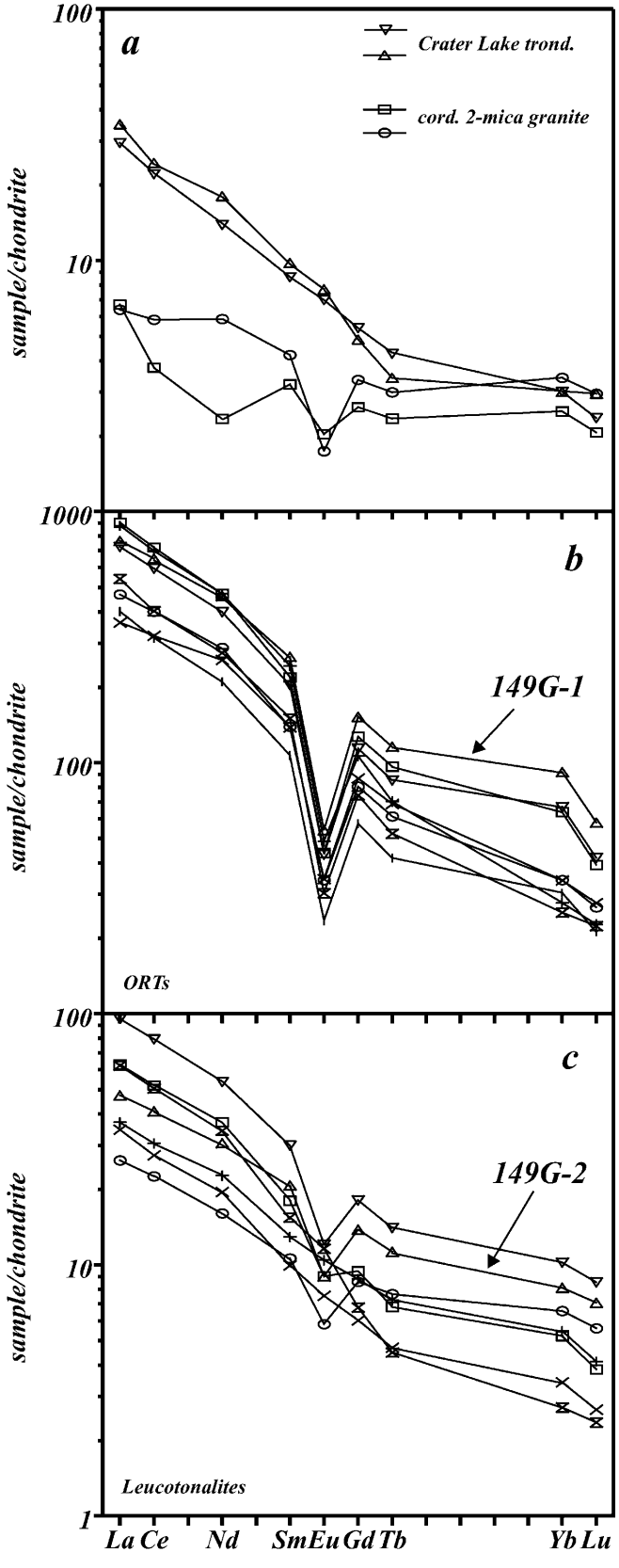

Fig. 4 Chondrite-normalized REE patterns for rocks from the Cornucopia stock. Chondrite normalization factors are those of Haskin et al. (1968). **a** Crater Lake trondhjemite and late-stage granitic dikes, both of which are cordierite + muscovite-bearing. **b** ORTs. **c** Leucotonalites. Hand-separated aliquots from sample 149G are indicated. Note the different logarithmic scale for comparison in **b**

P_2O_5, Rb, and Ta, and low Hf, Zr, and Sr (Fig. 3). Granitic compositions plot at the Al_2O_3-poor end of the trend displayed by Crater Lake trondhjemite compositions in each of the diagrams in Fig. 3. Values of A* for granitic rocks (8.00–8.67) are considerably higher than those for other lithologies. Granites are depleted in ΣREE (La_N = 6.4–6.7) and are characterized by relatively flat chondrite-normalized REE patterns [$(La/Lu)_N$ = 1.9–2.7] and negative Eu anomalies (Eu/Eu* = 0.59–0.70; Fig. 4a).

Isotopic data

Tonalitic and trondhjemitic rocks of the Cornucopia stock are characterized by low initial $^{87}Sr/^{86}Sr$ (0.7033–0.7035) and high ϵ_{Nd} (+5.8 to +6.1) and a narrow range of whole rock $\delta^{18}O$ values (+7.6 to +8.8‰; Johnson, unpublished data). Samples from the Crater Lake trondhjemite have whole rock $\delta^{18}O$ values of +8.2 and +8.3‰, and quartz from one sample yielded a $\delta^{18}O$ value of +9.6‰ (Table 2). Whole rock and quartz $\delta^{18}O$ values for leucotonalite samples (+8.2 to +8.5‰ and +9.1 to +9.6‰, respectively; Table 2) are similar to those of the Crater Lake unit. Granitic samples yield a range of whole rock $\delta^{18}O$ values from +8.4 to +9.5‰. One sample (sample 33) has an initial $^{87}Sr/^{86}Sr$ value of 0.7035, identical to the host trondhjemite (Johnson, unpublished data).

Quartz from ORT samples yields a narrow range of $\delta^{18}O$ values (+9.2 to +9.6‰), and biotite has values between +4.4 and +5.1‰ (Table 2). Calculated quartz–biotite isotope equilibrium temperatures for ORT samples range from 567 to 669 °C (mean temperature of 622 ± 36 °C), which represent near-solidus conditions. These temperatures are similar to amphibole–plagioclase solidus temperatures of 658 ± 29°C calculated for the Cornucopia stock (Johnson et al. 1997), using the algorithms of Blundy and Holland (1990), and Holland and Blundy (1994).

Biotite compositions

Average biotite compositions from the Crater Lake trondhjemite and two ORT samples are presented in Table 3. Biotite from the Crater Lake trondhjemite is similar to that from the other cordierite-bearing trondhjemitic units (Johnson 1995), and generally exhibits a relatively narrow range of compositions. However, biotite in the Crater Lake unit has higher Fe^{3+}/Fe_{total}

Table 3 Average biotite compositions. *n.d.* Not determined; *Mg#* molar Mg/(Mg + Fe total); *n* number of samples included in average and standard deviation

	Crater Lake trondhjemite				ORT			
	65		58		99B		127	
	Average	SD	Average	SD	Average	SD	Average	SD
Compositions in wt%								
SiO_2	35.33	0.34	35.76	0.46	35.49	0.66	35.52	0.31
TiO_2	2.97	0.18	2.79	0.18	2.62	0.01	2.58	0.33
Al_2O_3	17.37	0.43	17.32	0.33	18.08	0.42	18.84	0.50
FeO	19.16	0.67	18.03	0.63	17.33	1.54	16.97	0.87
MgO	10.14	0.33	10.58	0.18	10.73	0.72	9.87	0.25
BaO	0.13	0.11	0.40	0.24	0.77	0.14	0.76	0.22
K_2O	10.06	0.23	9.83	0.15	8.99	0.20	9.49	0.30
Cl	0.03	0.01	0.04	0.01	0.04	0.01	0.04	0.01
F	0.42	0.20	0.34	0.14	n.d.		n.d.	
Total	95.61	0.70	95.08	0.81	94.07	0.22	94.06	0.32
Less O	–0.18	0.09	–0.15	0.06	–0.01	0.00	–0.01	0.00
Total	95.43	0.71	94.93	0.80	94.06	0.22	94.06	0.32
Cations per 22 oxygens								
Si	5.393	0.046	5.457	0.021	5.442	0.055	5.444	0.038
Al^{iv}	2.607	0.046	2.543	0.021	2.558	0.055	2.556	0.038
Al^{vi}	0.518	0.037	0.572	0.043	0.711	0.082	0.849	0.086
Ti	0.341	0.020	0.320	0.019	0.303	0.004	0.297	0.039
Fe^{2+}	2.445	0.090	2.301	0.090	2.225	0.222	2.176	0.120
Mg	2.307	0.075	2.406	0.042	2.451	0.142	2.255	0.047
Ba	0.008	0.006	0.024	0.014	0.046	0.009	0.046	0.013
K	1.959	0.037	1.914	0.044	1.760	0.046	1.856	0.059
Cl	0.008	0.003	0.010	0.003	0.011	0.004	0.009	0.002
F	0.201	0.097	0.163	0.068				
Total	15.788	0.080	15.710	0.083	15.506	0.077	15.488	0.052
Al_{total}	3.125	0.066	3.115	0.030	3.269	0.051	3.404	0.076
Mg#	0.485	0.016	0.511	0.012	0.525	0.038	0.509	0.016
n	14		7		5		11	

(0.26) than biotite from the other units (0.15–0.22; Johnson 1995). Biotite in the cordierite-bearing trondhjemites exhibits a range in Al^{vi} from 0.40 to 0.68 atoms per formula unit (p.f.u.; Fig. 5). Biotite in the ORTs has Cl contents and $Mg/(Mg + Fe_{total})$ similar to those in the cordierite-bearing trondhjemites (Table 3 and Fig. 5), but is considerably higher in Al^{vi} (0.64 to 1.03 p.f.u.) and lower in Fe^{3+}/Fe_{total} (0.09; Johnson 1995).

Origin of the Cornucopia ORTs

The Cornucopia ORTs described here are similar to the oxide-rich segregations typical of anorthosite massifs because of their (1) obvious igneous intrusive nature, (2) enrichment in REE and HFSE abundances relative to host rocks, and (3) similar mineralogies and isotope compositions to that of the host pluton. These features suggest a cogenetic relationship between the oxide-rich accumulations and the host intrusive rocks.

A petrogenetic model for the Cornucopia ORTs must be consistent with a number of observations. (1) A genetic relationship exists between the ORTs, leucotonalites, and the cordierite trondhjemites. This is indicated by their similar mineralogy, particularly the presence of cordierite, and by similar mineral and whole rock $\delta^{18}O$ values. Furthermore, this occurrence is not unique: magnetite accumulations crop out at the margin of another body of cordierite trondhjemite in the Wallowa batholith (approximately 15 km to the northwest; Taubeneck 1987). Thus, the origin of the ORTs is apparently linked to the magmatic history of the cordierite trondhjemites. (2) Most ORTs in the Cornucopia stock were emplaced at the margin of the Crater Lake trondhjemite, either within the Crater Lake trondhjemite or in the adjacent Cornucopia tonalite. (3) They are typically associated with leucotonalite as composite dikes and sheets. (4) Biotite in the ORT samples is compositionally distinct from biotite in the cordierite-bearing trondhjemites, particularly in its higher Al^{vi} and lower Fe^{3+}/Fe_{total}. (5) Oxide-rich tonalites and leucotonalites have chondrite-normalized REE patterns with negative Eu anomalies, which indicates either that plagioclase was removed prior to their crystallization or that plagioclase was residual in the source. In the following discussion we investigate the origin of the ORTs in terms of various igneous and hydrothermal processes.

Hydrothermal processes

Chlorine-rich hypersaline fluids are capable of transporting iron in solution and depositing iron oxides in a

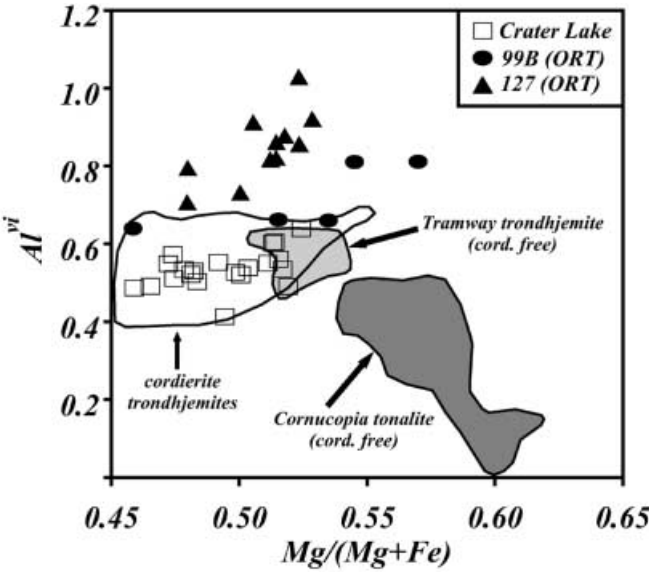

Fig. 5 Biotite compositions for rocks from the Cornucopia stock. *Shaded fields* represent compositions from the Cornucopia tonalite and Tramway trondhjemite, whereas *unshaded field* encompasses biotite compositions from the Pine Lakes, Big Kettle, and Crater Lake cordierite trondhjemites (see Johnson et al. 1997). Also included are individual biotite compositions from ORT samples 99B and 127, and Crater Lake trondhjemite samples 58 and 65

hydrothermal environment (Whitney et al. 1985; Rankin et al. 1992). Fluid inclusions in ORTs and leucotonalites are secondary, and consist of low to moderate salinity aqueous solution (5.6 ± 3.3 wt% NaCl equivalent) that homogenizes at < 330 °C (Johnson et al. unpublished data). In addition, deposition from Cl-rich fluid is not consistent with the low Cl contents of biotite in the ORTs and the lack of hydrothermal alteration, replacement textures, and other associated mineralization, commonly Cu–U–Au (Hildebrand 1986; Gow et al. 1994; Foose and McLelland 1995; Allen et al. 1996; Arancibia and Clark 1996; Barton and Johnson 1996).

Liquid immiscibility

Prior to the recognition of conjugate Fe-rich and Si-rich liquids as micrometer-size, quenched droplets in lunar and terrestrial basalts by Roedder and Weiblen (1971), evidence for liquid immiscibility was largely limited to experiments involving relatively simple synthetic systems (Greig 1927; Roedder 1951; Philpotts 1967). Philpotts (1967) determined a two-liquid field between dioritic and Fe- and P-rich conjugate liquids, and demonstrated that a eutectic exists with a proportion of magnetite to apatite of 2:1. Subsequent studies have underscored the similarity in magnetite and apatite proportions observed in nelsonitic rocks as evidence for liquid immiscibility (Badham and Morton 1976; Kolker 1982). However, silicate liquid immiscibility acting on a large scale has not been demonstrated convincingly in felsic calc-alkaline compositions.

The close association between ORT and leucotonalite in the composite dikes, and the elevated REE and HFSE abundances in the ORTs relative to the leucotonalites (Watson 1976; Ellison and Hess 1989), could be suggestive of immiscible separation of Fe- and Si-rich liquids. If this were the case, then the original parental liquid would have a composition intermediate between leucotonalitic and ORT end members. Crater Lake trondhjemite samples do not plot between ORT and leucotonalitic compositions, which indicates that leucotonalite and ORT cannot be immiscible pairs derived from a trondhjemitic parental magma. The Fe-rich immiscible end member should be strongly depleted in K_2O, Rb, and Ba, which is clearly at odds with the biotite-rich nature of the ORTs. Furthermore, experiments by Greig (1927) and Naslund (1976) indicated that immiscible liquid separation is suppressed in the presence of even minor amounts of Al_2O_3, which is not compatible with the strongly peraluminous compositions in the Crater Lake trondhjemite.

It could be argued that the REE-depleted, high K_2O granitic dikes in the Crater Lake trondhjemite represent the SiO_2-rich conjugate liquid to the leucotonalite/ORT magma. However, the granitic dikes were intruded after ORT emplacement; direct evidence of the coexistence of ORT and granitic magmas is lacking. Therefore, it seems unlikely that the extreme Fe-rich compositions seen in the Cornucopia stock were produced through the separation of an immiscible liquid.

Crystal fractionation and accumulation from evolving trondhjemite

Crystallization, separation, and accumulation of early-formed phases have been invoked to explain largely monomineralic segregation deposits, such as olivine and chromite layers in mafic and ultramafic layered intrusions (e.g., Wager and Brown 1968). This scenario necessarily implies that such minerals crystallize early in the magma's history, so that the magma's viscosity is low enough to allow migration and collection of solid crystals. Because of the lack of isotopic distinctions between the rocks under study, major element mass balance calculations (Bryan et al. 1969) were performed to determine if the ORTs in the Cornucopia stock might represent early magnetite (+biotite) cumulates from the Crater Lake trondhjemite as it evolved to more SiO_2-rich compositions. Mineral compositions used in the calculations are in Johnson (1995) and Johnson et al. (1997), with the exception of apatite (DeRosa 1992). Results of these calculations were considered viable if the sum of the squares of the residuals (*ssr*) was less than unity.

The first mass balance calculations to be considered are ones in which various ORT compositions are removed from the least siliceous Crater Lake trondhjemite to produce the most siliceous Crater Lake compositions. These calculations result in poor fits to the data, as

Table 4 Results of major element mass balance calculations (after Bryan et al. 1969). *F* Weight fraction of liquid remaining; *ssr* sum of the squares of the residuals; *LT* and *ORT* leucotonalitic and ORT end members, respectively; *X* mole fraction of anorthite component in plagioclase feldspar; *CLave* and *PLave* mean compositions of the Crater Lake and Pine Lakes trondhjemites, respectively (see Johnson et al. 1997)

Model	Parent	Plagio-clase	Quartz	Biotite	Cordierite	Ti–magnetite	Apatite	K-Feldspar	LT	ORT	Other	Daughter	*X*An	F	ssr	Samples
1A	58									0.009		65		0.957	4.532	ORT:149 G-1
1B	58								0.971	–0.088		65		0.129	0.284	LT: 155A; ORT: 155B
1C	58								0.224	–0.004		65		0.770	0.419	LT: 149G-2; ORT: 149G-1
2A	65	0.521	0.353		0.053							LT+ORT	0.24	0.065	0.942	
2B	65	0.516	0.348		0.053							155mix	0.24	0.076	0.918	
2C	CLave	0.579	0.331	0.082								LT+ORT	0.24	0.004	0.254	
2D	CLave	0.545	0.313	0.035	0.011			0.048				LT+ORT	0.24	0.042	0.041	
3A	CLave	0.487	0.254	0.023	0.026	0.009	0.002					107	0.24	0.191	0.001	
3B	PLave	0.531	0.265	0.043	0.015	0.009	0.003					33	0.24	0.127	0.008	

shown by the high *ssr* values >4.5 (model 1A using Fe-rich sample 149G-1; Table 4). Additional calculations attempted to explain the trend of Crater Lake compositions by removal of both ORT and leucotonalite compositions, owing to their close association in composite dikes. These models yielded acceptable *ssr* (0.284–0.509) only with the addition of ORT compositions, rather than their removal (models 1B, 1C). Thus, the ORTs and related leucotonalites could not have been the result of simple fractional crystallization of the Crater Lake trondhjemite.

Residual liquid separation

Separation of a late Fe-rich residual liquid was proposed by Bateman (1951) to explain the intrusive nature of oxide–apatite gabbronorites associated with anorthosite massifs. According to this idea, crystallization of large proportions of plagioclase enriches the residual liquid in such elements as Fe, Ti, and P. This dense residual liquid sinks to the base of the crystallized pile. It may be subsequently mobilized in response to differential stress, and can intrude other rocks or the partially solidified crystal mush of the overlying pile. The plagioclase-rich cumulate solidifies to form anorthosite, whereas the oxide–apatite gabbronorites are interpreted as the crystallized residual liquid itself (Ashwal 1982; Owens and Dymek 1992; McLelland et al. 1994) or as residual liquid-derived cumulates (Scoates et al. 1996; Vander Auwera et al. 1998).

The ORT-bearing magmas in the Cornucopia stock were emplaced late in its history (see above). Therefore, it is possible that ORT and leucotonalite represent the cumulate and fractionated liquid, respectively, of a residual, Fe-rich liquid that separated from a trondhjemitic parental magma. In the following section, we first address the proposed relationship between the ORT and leucotonalite compositions, and then discuss a residual liquid origin for the composite dike magmas from parental cordierite-bearing trondhjemites.

Bulk composition of the composite dikes

In Fig. 3a, ORT compositions extend toward higher SiO_2 and Al_2O_3, represented by sample 145B, which contains the highest modal abundances of plagioclase and quartz. This trend, if projected toward higher SiO_2 and Al_2O_3 compositions, intersects the range of leucotonalitic samples. Similar trends are observed with respect to most elements, with the exceptions of CaO (Fig. 3e) and Sr and Zr, which trend toward the felsic end of the leucotonalite range (Fig. 3d, f). If the ORTs represent magnetite-rich cumulates from an initial Fe-rich parental magma, then the leucotonalite compositions represent the resultant fractionated residual magma. In this case, plagioclase and quartz in the ORT samples would represent trapped crystals or magma

pockets that did not separate from the magnetite cumulate.

The original composition of a composite dike magma should plot along a line joining ORT and leucotonalitic compositions. Because of the ranges in leucotonalite and ORT compositions, estimating the original composition(s) of the composite dikes is problematic. Mass balance calculations between the two end members cannot determine their relative proportions. Therefore, some additional constraint is needed. Petrographic relationships show that cordierite crystallized early in the composite dike rocks, and that cordierite was in equilibrium with the ORT assemblage. Therefore, the ORTs (which have $A^* \ll 6.4$) crystallized from a strongly peraluminous magma. Mass balance calculations can be constrained so that the product of mixing ORT and leucotonalite compositions is strongly peraluminous ($A^* = 6.4$). Because the parental magma may have had $A^* > 6.4$, this constraint results in an estimate of the *maximum* fraction of ORT that can be added to leucotonalite.

The compositions of various ORT and leucotonalite mixtures were calculated by adding variable proportions of the two end members together. As a first approximation, a parental liquid composition was calculated by choosing the mean compositions of ORT and leucotonalite end members (LT + ORT). These results are compared with results of calculations in which ORT and leucotonalite compositions from individual composite dikes were used (Table 5). Calculated ORT fractions (X_{ORT}) range from 0.208 to 0.518. The highest X_{ORT} value of 0.518 is for sample 145B, which contains more plagioclase and quartz than the other ORT samples. Despite the wide range in X_{ORT} values, the calculated Fe-rich liquid compositions for all the mixtures (1) exhibit a relatively narrow range in most major and trace element abundances (Table 5), (2) are all quartz-normative, and (3) exhibit nearly identical chondrite-normalized REE patterns (Fig. 6). Of particular note are the high Fe contents of the calculated residual liquid (14.45 to 20.88 wt% FeO) and their low CaO (< 3 wt%), which contributes to their strongly peraluminous nature.

Table 5 Calculated compositions of the Fe-rich residual liquids. X_{ORT} Fraction of ORT in the calculated composition. Major elements are in wt%, trace elements are in ppm. Samples *145mix*, *155mix*, and *149Gmix* were calculated using ORT and leucotonalite compositions from the same composite dikes; *LT + 149G-1* represents a calculated mixture of average leucotonalite and sample 149G-1, the most Fe-rich ORT; *LT + ORT* is the calculated mixture of average leucotonalite and ORT compositions

	145mix	155mix	149Gmix	LT + 149G-1	LT + ORT
SiO_2	52.97	57.95	50.72	55.03	55.44
TiO_2	1.01	0.94	0.85	0.93	0.93
Al_2O_3	12.67	14.13	18.36	14.54	14.58
FeO	20.88	14.45	17.46	17.73	16.71
MnO	0.34	0.29	0.46	0.39	0.33
MgO	0.74	0.89	1.52	0.92	0.95
CaO	1.58	2.28	3.54	2.36	2.46
Na_2O	3.94	4.55	3.81	4.35	4.42
K_2O	1.69	1.14	0.57	1.07	1.15
P_2O_5	0.19	0.14	0.14	0.19	0.27
Total	96.01	96.76	97.43	97.51	97.24
Sc	7.6	6.8	5.0	6.3	6.1
Rb	23	18	7	15	17
Sr	398	521	703	542	542
Ba	829	595	292	574	602
Y	38.3	41.2	55.1	57.0	35.2
La	73.9	74.7	63.4	69.3	65.0
Ce	154.0	163.4	144.3	156.5	141.4
Nd	70.9	74.9	70.6	75.7	66.9
Sm	10.9	12.0	12.6	13.0	10.6
Eu	1.1	1.3	1.2	1.3	1.2
Tb	1.1	1.4	1.5	1.5	1.2
Yb	3.5	4.4	5.0	5.0	3.2
Lu	0.4	0.5	0.6	0.6	0.4
X_{ORT}	0.518	0.208	0.202	0.222	0.251

Because the major element compositions of the ORT and leucotonalite end members were used to calculate the composition of the parental composite dike magmas, a fractional crystallization origin for the ORTs (as opposed to a liquid–liquid separation mechanism) cannot be evaluated with the major element data. Fractional crystallization was tested using a strongly compatible trace element (Sc) and a strongly incompatible trace element (Sr). The bulk distribution coefficients for these elements were determined using the modal mineralogy of the most magnetite-rich ORT (sample 149G; Table 1), which we used as a proxy for the most primitive cumulate. The parental magma used in these calculations is LT + ORT (calculated mixture of average leucotonalite and ORT compositions; Table 5). In Fig. 7, the curve representing residual liquid compositions produced by fractional crystallization (curve FC) passes through a field containing most of the leucotonalitic rocks. Similarly, the bulk cumulate represented by curve BC passes through the field of ORT compositions at values of F (weight fraction of liquid remaining) between 0.50 and 0.80, which correspond to X_{ORT} values of 0.50 to 0.20, respectively. These X_{ORT} values are very similar to those predicted by mass balance mixing calculations (Table 5), and support the idea that ORT and leucotonalite samples represent cumulates and residual liquids, respectively, from an Fe-rich parental magma. In light of this interpretation, cumulates at lower F values might reflect incomplete separation of tonalitic residual liquid from the accumulating assemblage.

Formation of Fe-rich residual liquid

The low SiO_2 contents of the calculated composite dike magmas, relative to the trondhjemitic host rocks, indicate that if the Fe-rich magma formed by fractional crystallization from the trondhjemites, then the cumulate must have been SiO_2-rich. The negative Eu anomalies in both ORT and leucotonalite samples also show that the proposed cumulate was rich in plagioclase. Major element mass balance calculations show that removal of a solid assemblage of 51–55% plagioclase (An_{19-24}) + 33–35% quartz + ~5% cordierite from the

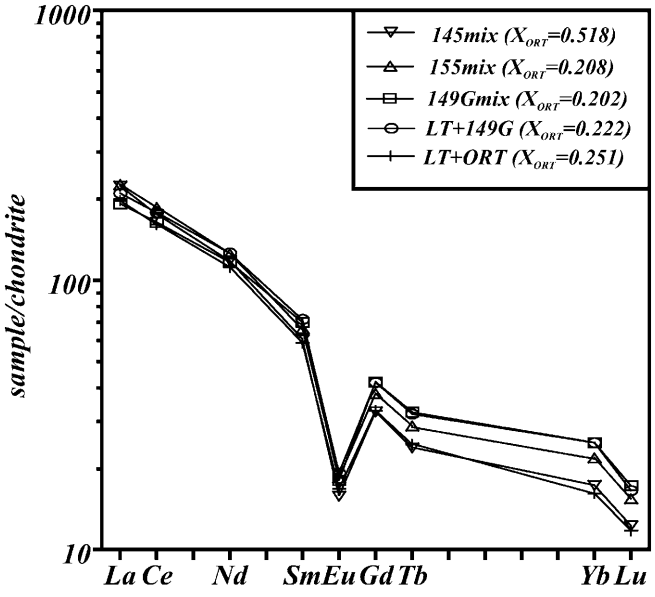

Fig. 6 Chondrite-normalized REE patterns for the calculated Fe-rich residual liquid (see text). Included are the calculated fractions of ORT (X_{ORT}) in each ORT + leucotonalite composite dike. Note the similar REE patterns calculated for the Fe-rich residual liquid, despite the wide range in X_{ORT}

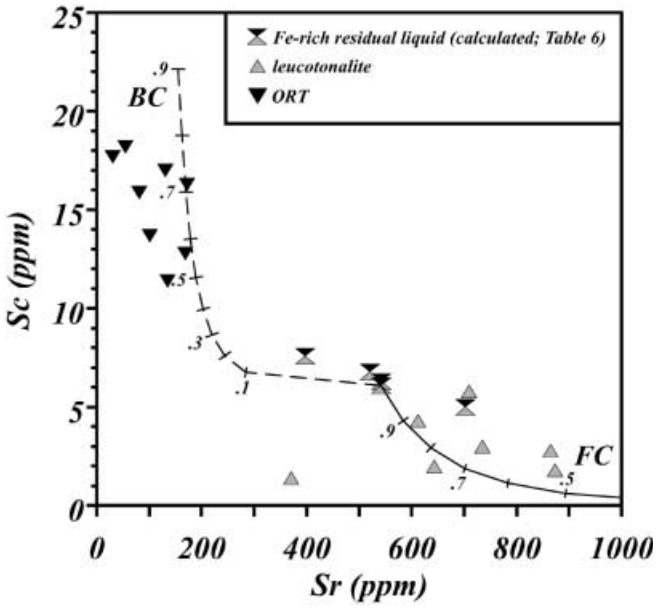

Fig. 7 Graph of Sc versus Sr showing curves representing the compositions of the bulk cumulate (*dashed curve* BC) and resultant derivative liquid (*solid curve* FC) produced by fractional crystallization from an Fe-enriched magma. Numbers adjacent to curves denote melt fractions (i.e., 1.0–X_{ORT}). Settling and accumulation of the magnetite + biotite-rich assemblage led to the composite dike relationships shown in Fig. 2d, e

Crater Lake trondhjemite results in a small fraction (6–8 wt%) of Fe-enriched residual liquid (models 2A, 2B; Table 4). However, successful results were only accomplished with the most siliceous of the Crater Lake trondhjemite samples (sample 65). Additional models in which ~8 wt% biotite is also removed from the average Crater Lake trondhjemite (model 2C) result in a very small fraction of residual liquid (< 1 wt%). Models in which K-feldspar is also a fractionating phase allow for both cordierite and biotite to be removed from the average Crater Lake trondhjemite, and result in the lowest *ssr* values (0.041; model 2D). The results of this model yield ~4 wt% residual Fe-rich liquid. The presence of K-feldspar in the fractionating assemblage suggests that the Fe-rich residual magma formed very late in the crystallization history of the Crater Lake trondhjemite. None of the successful models allowed for magnetite fractionation.

Successful major element results were tested with calculations using Sr, Sc, Y, Rb, and REE abundances. These elements were chosen because of their relative immobility (Sc, Y, and REEs) and incorporation into plagioclase (Sr) and biotite (Rb and Sc), which are important phases in our petrogenetic interpretation for the ORTs. Trace element bulk distribution coefficients were determined using the mineral proportions from the major element results (Table 4) and the mineral/liquid partition coefficients in Table 6.

Table 6 Mineral/liquid partition coefficients used in geochemical modelling. Sources: *1* Nash and Crecraft (1985); *2* Mahood and Hildreth (1983); *3* Arth (1976); *4* Broeker and Peng (1982); *5* Bea et al. (1994b); *6* Watson and Green (1981); *7* Ewart and Griffin (1994)

	Plagioclase	Biotite	K-Feldspar	Ti oxides	Apatite	Quartz	Cordierite
Rb	0.048	3.2	0.34	0.01		0.041	0.08
Sr	4.4	0.447	3.87	0.01	2.4		0.12
Sc	0.053	4.9	0.04	5		0.012	2.05
Y	0.13	1.233	0.086	2	40		0.72
La	0.38	3.18	0.072	0.66		0.015	0.06
Ce	0.267	2.803	0.046	0.71	34.7	0.014	0.07
Nd	0.203	2.233	0.038	0.93	57.1	0.016	0.09
Sm	0.165	1.55	0.025	1.2	62.8	0.014	0.1
Eu	5.417	0.867	2.6	0.91	30.4	0.056	0.01
Gd	0.125				56.3		0.29
Tb		1.053	0.033	1.3		0.017	0.95
Yb	0.09	0.537	0.015	0.44	23.9	0.017	1.77
Lu	0.092	0.613	0.031	0.3	20.2	0.014	4.43
Sources	1, 3	1, 2	2, 3, 7	3, 4	3, 6	1	5

Perfect Rayleigh fractionation models (Fig. 8) predict high abundances of Sc (~20 ppm) and Y (~200 ppm), and low abundances of Sr (< 30 ppm) in the residual liquid for the low values of F required by the major element results (< 0.05). Clearly, such values are far from the calculated compositions of the Fe-rich residual magmas. As an alternative to pure Rayleigh fractionation, attempts were made to explain the data in terms of in-situ crystallization (Langmuir 1989; Srogi and Lutz 1996), whereby a certain proportion of the residual liquid evolves in equilibrium with the cumulate framework. In-situ crystallization results in less pronounced enrichment of incompatible elements and depletion of compatible elements compared with fractional crystallization. This is because only a fraction of the residual liquid (denoted *f*) is returned to the magma chamber from the zone of crystallization (Langmuir 1989).

In-situ crystallization calculations using the mineral proportions in model 2D (with 3.5 wt% biotite) are broadly consistent with the observed Sr, Sc, and Y abundances of the calculated Fe-rich residual liquid (Fig. 8). These calculations predict that a relatively large fraction (0.70–0.90) of the residual liquid remained in equilibrium with the cumulate assemblage. Similarly, in-situ calculations using cordierite as the sole ferromagnesian phase (models 2A, 2B) also yield acceptable results (not shown). In contrast, calculations in which biotite is the fractionating ferromagnesian phase (model 2C) result in a bulk distribution coefficient for Sr that is too high ($D^{Sr} = 2.58$; Fig. 8b).

Figure 9 shows the results of Rayleigh fractionation and in-situ crystallization calculations using the REEs. Rayleigh fractionation results in chondrite-normalized patterns that are similar in shape to the calculated Fe-rich residual liquid, but with higher REE abundances and a very deep negative Eu anomaly. The large degree of Eu depletion in these calculations is a function of using plagioclase partition coefficients from high-Si rhyolite (Table 6), which may not be appropriate for the compositions discussed here. Although not a perfect match, the REE pattern predicted by in-situ crystallization more closely resembles the pattern of the calcu-

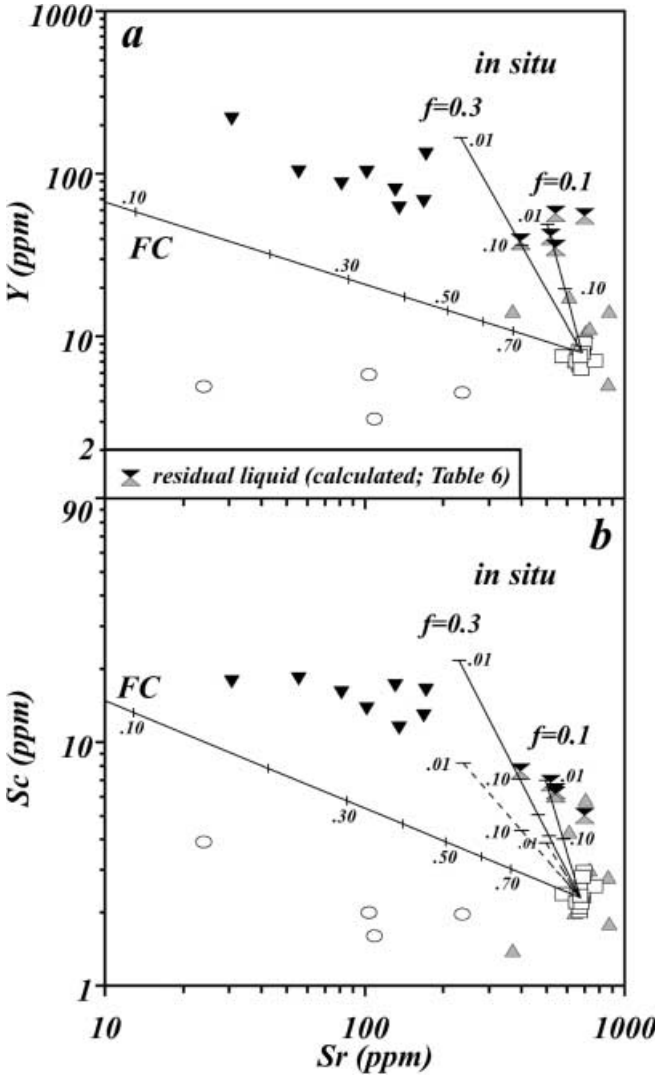

Fig. 8 Fractional crystallization (*FC*) and in-situ crystallization curves calculated from results of major element mass balance models (Table 4), for the generation of Fe-rich residual liquid from fractionating trondhjemitic magma. The *solid curves* representing in-situ crystallization encompass the field of calculated Fe-rich residual liquids (see Table 5) for values of *f* between 0.1 and 0.3 (*f* is the weight fraction of liquid returned to the magma chamber from the zone of crystallization). *Numbers adjacent to curves* denote melt fractions (*F*). *Dashed curves* in **b** represent in-situ crystallization ($f = 0.1$ and 0.3) based on model 2C (biotite as sole ferromagnesian phase). See text for discussion. *Symbols* as in Fig. 3

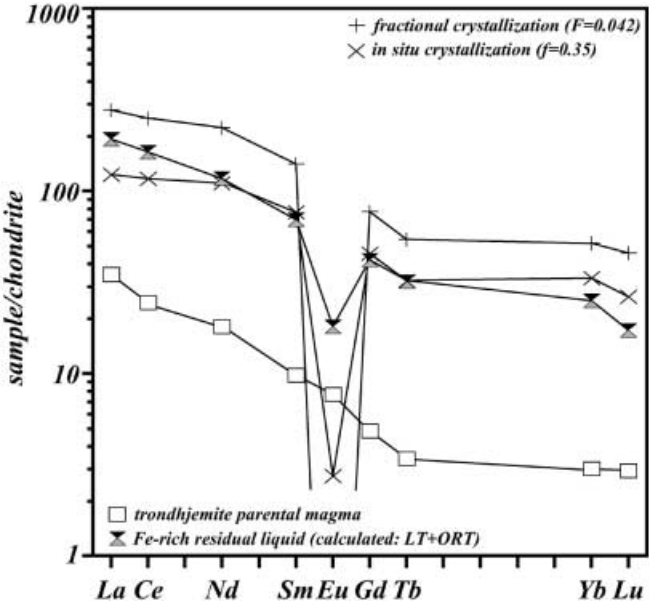

Fig. 9 Calculated rare earth element patterns for fractional crystallization and in-situ crystallization from results of major element mass balance models (Table 4), for the generation of Fe-rich residual liquid from a fractionating trondhjemitic magma. Also shown are the patterns representing the trondhjemitic parental magma (sample 84) and the calculated Fe-rich residual liquid (LT + ORT; Table 5 and Fig. 6)

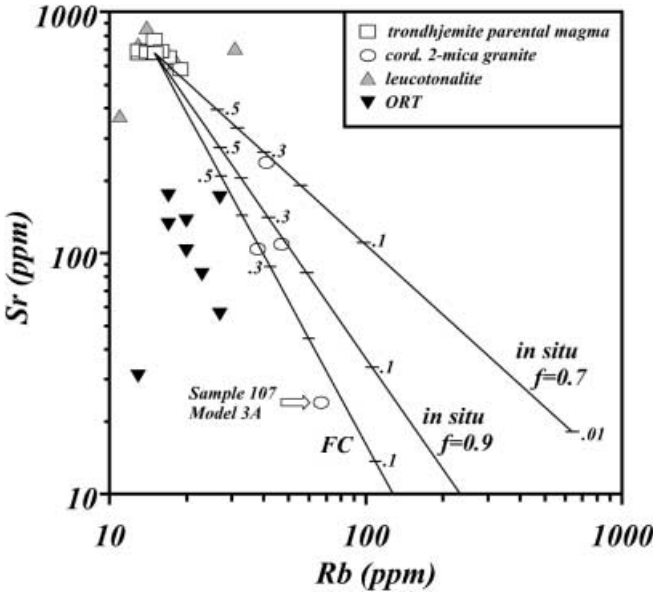

Fig. 10 Fractional crystallization (*FC*) and in-situ crystallization curves calculated from results of major element mass balance models (Table 4) for the generation of granitic liquid from fractionating trondhjemitic magma. The *curves* encompass the field of granitic compositions (see Table 2) for values of *f* between 0.7 and 1.0 (i.e., *FC*). *Numbers adjacent to curves* denote melt fractions (*F*). Values of *F* calculated for fractional crystallization more closely match those derived from major element models (Table 4), whereas in-situ crystallization requires slightly greater *F* values

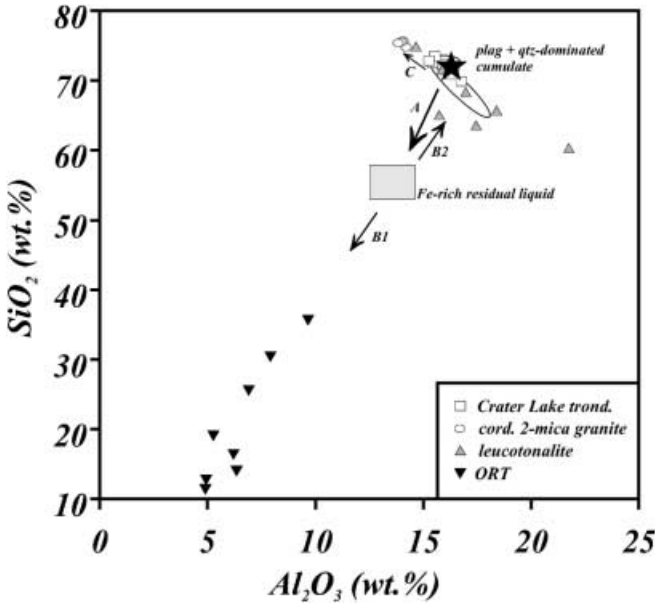

Fig. 11 Variation of Al_2O_3 and SiO_2, illustrating the possible stages in the origin of the ORTs in the Cornucopia stock. In-situ crystallization of a strongly peraluminous trondhjemitic magma formed a plagioclase + quartz-dominated solid cumulate (*solid black star*) and an Fe-rich residual liquid (*arrow A*). Fractional crystallization of the Fe-rich liquid led to a magnetite + biotite-rich cumulate (ORTs; *arrow B1*) and a tonalitic derivative magma (leucotonalites; *arrow B2*). Late-stage granitic magma was formed by fractional crystallization of strongly peraluminous trondhjemite (*arrow C*; see text). *Solid curve* outlines the compositions of tonalitic and trondhjemitic rocks in the Cornucopia stock

lated Fe-rich residual liquid, especially the middle REEs, for an *f* value of 0.35. This *f* value is only slightly higher than those predicted by the other trace elements.

Thus, an origin for the magma parental to the ORT and leucotonalitic compositions as residual liquid from plagioclase-dominated crystallization is consistent with major, trace, and rare earth elements. The model requires early crystallization of predominantly plagioclase and quartz from strongly peraluminous trondhjemite, with consequent small fractions of residual liquid and enrichment of Fe, P, and the other elements excluded from the crystalline framework. The success of in-situ crystallization models implies that a significant fraction of residual melt remained in equilibrium with the crystalline mush, which is consistent with the uniform $\delta^{18}O$ values of quartz amongst all lithologies.

Although these results demonstrate a possible mechanism by which the Fe-rich composite dike magmas could form, specific details should be viewed with caution. Uncertainties inherent in the calculations include errors associated with recalculating composite dike magma compositions (see discussion above), use of appropriate mineral/liquid partition coefficients, and the effects of accessory phases on Sc, Y, and REE abundances. Nevertheless, the results demonstrate the viability of in-situ crystallization to produce Fe-rich composite dike magmas followed by fractional crystallization of the Fe-rich composite dike magmas to form the ORTs.

Origin of late-stage granites

Late-stage granites are a ubiquitous feature of high-Al TTG suites, which suggests their association is not fortuitous and that generation of K-rich liquids is in some way associated with tonalite–trondhjemite magmatism. Fractional crystallization of tonalitic–trondhjemitic magma is commonly invoked to explain the small volumes of late-stage granitic dikes in TTG suites (Rollinson and Windley 1980; Luais and Hawkesworth 1994). Late-stage felsic dikes in the Cornucopia stock have identical mineralogies to their host plutonic rocks. Mildly peraluminous biotite ± hornblende tonalite and biotite trondhjemite (the Cornucopia tonalite and Tramway trondhjemite) contain dikes of biotite granodiorite, whereas dikes of cordierite two mica granite are only present in the strongly peraluminous cordierite two mica Pine Lakes and Crater Lake trondhjemites. Similarities in mineralogy between granitic dike and host pluton preclude an origin by wallrock anatexis. Instead, these distinct occurrences argue for a cogenetic relationship between the late-stage felsic liquids and their silicic hosts, which is consistent with their nearly identical initial $^{87}Sr/^{86}Sr$ and ϵ_{Nd} values.

Granitic dikes in the Crater Lake trondhjemite are characterized by high P_2O_5 contents and strong depletions in REE. Low REE abundances in such granites are

typical of monazite fractionation (Yurimoto et al. 1990; Bea et al. 1994a). Major element mass balance calculations suggest that the granitic dike compositions represent small fractions of liquid (< 20%) resulting from removal of plagioclase (An_{24}) + quartz + biotite + cordierite + magnetite ± apatite (monazite?) by crystallization differentiation of the Crater Lake or Pine Lakes trondhjemites (models 3A, 3B; Table 4). Successful results ($ssr < 1$) require magnetite in the fractionating mineral assemblage. Trace element tests of the mass balance calculations are generally consistent with major element results (Fig. 10) and support the idea that late-stage granitic dikes in the Cornucopia stock were derived from strongly peraluminous trondhjemitic magma. However, the unit from which they were derived (Crater Lake or Pine Lakes) cannot yet be resolved. Elevation of P_2O_5 in the granitic liquid might have resulted from minor wall rock interaction because the solubility of phosphorus is greatly increased in strongly peraluminous liquids (Wolf and London 1994). Minor assimilation is also consistent with the slightly higher $\delta^{18}O$ values in the granites, relative to the trondhjemites.

Discussion

Separation of Fe-enriched residual liquid is the most reasonable explanation for the composite dikes in the Crater Lake trondhjemite. It is consistent with the field relationships, mineralogy, oxygen isotope compositions, and the results of major and trace element calculations. Figure 11 illustrates the possible sequence of stages involved in the formation of the ORTs in the Cornucopia stock: (1) in situ crystallization of a plagioclase + quartz-rich solid assemblage (indicated by the solid star in Fig. 11) from a strongly peraluminous trondhjemitic magma resulted in the formation of Fe-enriched residual magma (arrow A). This Fe-rich magma was emplaced late in the crystallization history of the Crater Lake trondhjemite. (2) Fractional crystallization of the Fe-rich residual magma led to magnetite + biotite-rich cumulates (the ORTs; arrow B1) and tonalitic derivative magmas (leucotonalites; arrow B2), which are locally preserved as composite dikes. Incomplete separation of the intercumulus tonalitic liquid resulted in the observed range of ORT compositions. The higher Al^{vi} and Fe^{2+} in biotite of the ORTs, relative to biotite in the Crater Lake trondhjemite, probably reflects the fact that magnetite crystallization removed Fe^{3+} from the melt so that Al and Fe^{2+} were required to fill octahedral sites in the biotite.

It is difficult to reconcile the derivation of an Fe-rich residual liquid and an Fe-poor, silica-rich granitic liquid from the same parental magma by similar crystal–liquid separation processes. A trend of Fe-enrichment, as proposed here, demands that magnetite saturation be suppressed until late in the crystallization history of the magma, whereas early magnetite fractionation was involved in the generation of the granitic magmas. Another puzzling aspect of this scenario is that ORTs are associated only with the Crater Lake unit, and apparently not with the other cordierite-bearing trondhjemites in the Cornucopia stock.

If both the Fe-rich composite dikes and the granitic dikes were derived from the Crater Lake trondhjemite, then two different crystallization trends affected different parts of the same magma; one trend resulted in low SiO_2, high Fe residual liquid and the other produced high SiO_2, low Fe granite. Close proximity of the composite dikes to the margin of the Crater Lake unit suggests that the Fe^{3+}/Fe_{total} of the trondhjemitic magma might have been lower along the pluton's periphery. This would have the effect of suppressing magnetite saturation and could permit development of the Fe-rich composite dike magmas. Localized lowering of a magma's Fe^{3+}/Fe_{total} can result from interaction of the magma with graphite-bearing, or similarly reducing, metasedimentary wallrocks. A similar explanation was invoked for the low modal iron oxide content and low Fe^{3+}/Fe_{total} in a tonalitic pluton within the Bald Mountain batholith, also in the Blue Mountains (Taubeneck 1995). If this were the case, then it suggests that the magma was not well-mixed, so as to preserve the zonation in Fe^{3+}/Fe_{total}, and that the Crater Lake magma ascended through a different conduit than the other Cornucopia magmas, which show no such similar affects. It should be noted, however, that this interpretation is not consistent with other geochemical characteristics that are indicative of interaction with adjacent wallrocks (e.g., higher initial $^{87}Sr/^{86}Sr$, $\delta^{18}O$, and LILE abundances).

If, on the other hand, the Crater Lake trondhjemite was parental only to the Fe-rich composite dike magmas, then magnetite crystallization might have been suppressed as a result of lower total Fe, lower Fe^{3+}/Fe_{total}, or both throughout the magma body. The Mg-rich nature of cordierite and the higher Fe^{3+}/Fe_{total} in biotite in the Crater Lake trondhjemite argue against a low magmatic Fe^{3+}/Fe_{total}. However, the Crater Lake trondhjemite is, on average, lower in total Fe than the other units in the Cornucopia stock. Major element mass balance calculations indicate that cordierite and/or biotite crystallized with plagioclase and quartz, and if the magma had a total Fe content below that required for magnetite saturation, then the melt could have become enriched in iron compared with typical calc-alkaline suites. In the slightly more Fe-rich Pine Lakes trondhjemite, early magnetite crystallization might have been a response to a decrease in the melt Mg/Fe as a result of crystallizing Mg-rich cordierite. This scenario suggests the granitic dikes arose from the adjacent, more Fe-rich Pine Lakes trondhjemite, rather than the more Fe-poor Crater Lake trondhjemite.

Results of geochemical calculations suggest that the fractions of residual liquid produced by in-situ crystallization were very low (~4 wt%), too low probably for the melt to separate from the crystalline framework on its own. The mutual crosscutting relationships between shear zones and ORT-bearing composite dikes indicate

that the margin of the pluton was undergoing shear at the time of dike emplacement. We suggest that deformation related to shearing was probably necessary to mobilize the extremely small volumes of Fe-rich residual liquid. The abundance of biotite in the ORTs and the nearly anhydrous mineral assemblage (plagioclase + quartz) required to generate the Fe-rich residual liquid suggest that H_2O would have been enriched in the composite dike magma. This would have had the effect of lowering the solidus temperature and viscosity of the residual liquid and, combined with the deformation of the host trondhjemite, would have facilitated mobilization and emplacement.

The model for ORT generation in the Crater Lake trondhjemite is similar to the mechanism proposed by Scoates et al. (1996) for the formation of Fe-rich rocks in the Laramie anorthosite complex. In their study, extensive crystallization of anorthosite resulted in a ferrodioritic residual magma, which then underwent further crystallization to produce monzodioritic/monzonitic magma and Fe- and Ti-rich cumulates. Their model explained the trends in Fe-rich compositions that are orthogonal to the main crystallization trend of the anorthosite complex, similar to the orthogonal trends observed in the Cornucopia data. This suggests that conditions in normally oxidized trondhjemitic (or other siliceous) magmas may locally mimic the low fO_2 conditions of anorthosite massifs and can result in similar trends of Fe-enrichment. Similar oxide accumulations in other felsic intrusions, for which a mechanism of Fe-enrichment is uncertain (e.g., Reid et al. 1993), may result from similar processes.

Acknowledgements We thank the owners of the Cornucopia Wilderness Pack Station, Inc. for packing samples out of remote areas. Instrumental neutron activation analyses were provided by the Radiation Center at Oregon State University through the US Department of Energy Reactor Sharing Program. We thank Kip Miller for help with microprobe analyses, and Sharla Salisbury, Joel Boyd, Josh Rodgers, Shannon McGuire, and Melanie Barnes for assistance with sample preparation and ICP-AES analyses. The thorough and constructive comments of two anonymous reviewers are greatly appreciated. Funding for portions of this study were provided to K.J. by the Oregon Department of Geology and Mineral Industries, a Penrose Bequest of the Geological Society of America, and a Sigma Xi Grant-in-Aid of Research, and to C.G.B. through NSF grant EAR-9117103.

References

Allen RL, Lundström I, Ripa M, Simeonov A, Christofferson H (1996) Facies analysis of a 1.9 Ga, continental margin, back-arc, felsic caldera province with diverse Zn–Pb–Ag–(Cu–Au) sulfide and Fe oxide deposits, Bergslagen Region, Sweden. Econ Geol 91:979–1008

Arancibia ON, Clark AH (1996) Early magnetite–amphibole–plagioclase alteration-mineralization in the Island Copper Porphyry copper–gold-molybdenum deposit, British Columbia. Econ Geol 91:402–438

Arth JG (1976) Behavior of trace elements during magmatic processes – a summary of theoretical models and their applications. US Geol Surv J Res 4:41–47

Ashwal LD (1982) Mineralogy of mafic and Fe–Ti oxide-rich differentiates of the Marcy anorthosite massif, Adirondacks, New York. Am Mineral 67:14–27

Badham JPN, Morton RD (1976) Magnetite–apatite intrusions and calc-alkaline magmatism, Camsell River, NWT. Can J Earth Sci 13:348–354

Barker F (1979) Trondhjemite: definition, environment, and hypotheses of origin. In: Barker F (ed) Trondhjemites, dacites, and related rocks. Elsevier, New York, pp 1–12

Barton MD, Johnson DA (1996) Evaporitic-source model for igneous-related Fe oxide–(REE–Cu–Au–U) mineralization. Geology 24:259–262

Bateman AM (1951) The formation of late magmatic oxide ores. Econ Geol 46:404–426

Bea F, Pereira MD, Corretgé LG, Fershtater GB (1994a) Differentiation of strongly peraluminous, perphosphorus granites: the Pedrobernardo pluton, central Spain. Geochim Cosmochim Acta 58:2609–2627

Bea F, Pereira MD, Stroh A (1994b) Mineral/leucosome trace element partitioning in a peraluminous migmatite (a laser ablation–ICP–MS study). Chem Geol 117:291–312

Blundy JD, TJB Holland (1990) Calcic amphibole equilibria and a new amphibole–plagioclase geothermometer. Contrib Mineral Petrol 104:208–224

Broeker WS, Peng T-H (1982) Tracers in the sea. Eldigio Press, Palisades, New York

Bryan WB, Finger LW, Chayes F (1969) Estimating proportions in petrographic mixing equations by least squares approximation. Science 163:926–927

Clayton RN, Mayeda T (1963) The use of bromine pentafluoride in the extraction of oxygen from oxides and silicates for isotopic analysis. Geochim Cosmochim Acta 27:43–52

DeRosa ML (1992) Characterization of a zoned pluton with implications for intrusion and magmatic processes: Cornucopia stock, Wallowa Mountains, northeastern Oregon. MSc Thesis, University of Washington, Seattle

Drummond MS, Defant MJ (1990) A model for trondhjemite–tonalite–dacite genesis and crustal growth via slab melting: Archean to modern comparisons. J Geophys Res 95:21503–21521

Duchesne JC (1999) Fe–Ti deposits in Rogaland anorthosites (south Norway): geochemical characteristics and problems of interpretation. Miner Deposita 34:182–198

Ellison AJG, Hess PC (1989) Solution properties of rare earth elements in silicate melts: inferences from immiscible liquids. Geochim Cosmochim Acta 53:1965–1974

Ewart A, Griffin WL (1994) Application of proton-microprobe data to trace element partitioning in volcanic rocks. Chem Geol 117:251–284

Foose MP, McLelland JM (1995) Proterozoic low-Ti iron-oxide deposits in New York and New Jersey: relation to Fe-oxide (Cu–U–Au–rare earth element) deposits and tectonic implications. Geology 23:665–668

Frietsch R (1978) On the magmatic origin of iron ores of the Kiruna type. Econ Geol 73:478–485

Getty SR, Selverstone J, Wernicke BP, Jacobsen SB, Aliberti E, Lux DR (1993) Sm–Nd dating of multiple garnet growth events in an arc-continent collision zone, northwestern US Cordillera. Contrib Mineral Petrol 115:45–57

Gow PA, Wall VJ, Oliver NHS, Valenta RK (1994) Proterozoic iron oxide (Cu–U–Au–REE) deposits: further evidence of hydrothermal origins. Geology 22:633–636

Greig JW (1927) Immiscibility in silicate melts. Am J Sci 13:1–44, 133–154

Grez E, Aguilar A, Henríquez F, Nyström JO (1991) Magnetita Pedernales: a new magmatic iron deposit in northern Chile. Econ Geol 86:1346–1349

Haskin LA, Haskin MA, Frey FA, Wildeman TR (1968) Relative and absolute abundances of the rare earths. In: Ahrens LH (ed) Origin and distribution of the elements. Pergamon Press, Oxford, pp 889–912

Hildebrand RS (1986) Kiruna-type deposits: their origin and relationship to intermediate subvolcanic plutons in the Great

Bear magmatic zone, northwest Canada. Econ Geol 81:640–659
Holland T, Blundy J (1994) Non-ideal interactions in calcic amphiboles and their bearing on amphibole–plagioclase thermometry. Contrib Mineral Petrol 116:433–447
Johnson K (1995) Petrogenesis of high-alumina tonalite and trondhjemites of the Cornucopia stock, Blue Mountains, northeastern Oregon. PhD Thesis, Texas Tech University, Lubbock
Johnson K, Barnes CG, Miller CA (1997) Petrology, geochemistry, and genesis of high-Al tonalite and trondhjemites of the Cornucopia stock, Blue Mountains, northeastern Oregon. J Petrol 38:1585–1611
Kolker A (1982) Mineralogy and geochemistry of Fe–Ti oxide and apatite (nelsonite) deposits and evaluation of the liquid immiscibility hypothesis. Econ Geol 77:1146–1158
Langmuir CH (1989) Geochemical consequences of in situ crystallization. Nature 340:199–205
Luais B, Hawkesworth CJ (1994) The generation of continental crust: an integrated study of crust-forming processes in the Archean of Zimbabwe. J Petrol 35:43–93
Lundberg B, Smellie JAT (1979) Painirova and Mertainen iron ores: two deposits of the Kiruna iron ore type in northern Sweden. Econ Geol 74:1131–1152
Mahood GA, Hildreth EW (1983) Large partition coefficients for trace elements in high-silica rhyolites. Geochim Cosmochim Acta 47:11–30
McLelland J, Ashwall L, Moore L (1994) Composition and petrogenesis of oxide-, apatite-rich gabbronorites associated with Proterozoic anorthosite massifs: examples from the Adirondack Mountains, New York. Contrib Mineral Petrol 116: 225–238
Nash WP, Crecraft HR (1985) Partition coefficients for trace elements in silicic magmas. Geochim Cosmochim Acta 49: 2309–2322
Naslund HR (1976) Liquid immiscibility in the system $KAlSi_3O_8$–$NaAlSi_3O_8$–FeO–Fe_2O_3–SiO_2 and its application to natural magmas. Carnegie Inst Year Book 75:592–597
Nyström JO, Henríquez F (1994) Magmatic features of iron ores of the Kiruna type in Chile and Sweden: ore textures and magnetite geochemistry. Econ Geol 89:820–839
Owens BE, Dymek RF (1992) Fe–Ti–P-rich rocks and massif anorthosite: problems of interpretation illustrated from the Labrieville and St-Urbain plutons, Quebec. Can Mineral 30:163–190
Patiño Douce AE (1992) Calculated relationships between activity of alumina and phase assemblages of silica-saturated igneous rocks: petrogenetic implications of magmatic cordierite, garnet, and aluminosilicate. J Volcanol Geotherm Res 52:43–63
Philpotts AR (1967) Origin of certain iron–titanium oxide and apatite rocks. Econ Geol 62:303–315
Philpotts AR (1982) Compositions of immiscible liquids in volcanic rocks. Contrib Mineral Petrol 80:201–218
Rankin AH, Ramsey MH, Coles B, Van Langevelde F, Thomas CR (1992) The composition of hypersaline, iron-rich granitic fluids based on laser-ICP and Synchrotron-XRF microprobe analysis of individual fluid inclusions in topaz, Mole granite, eastern Australia. Geochim Cosmochim Acta 56:67–79
Reid JB, Murray DP, Hermes OD, Steig EJ (1993) Fractional crystallization in granites of the Sierra Nevada: how important is it? Geology 21:587–590
Ripley EM, Severson MJ, Hauck SA (1998) Evidence for sulfide and Fe–Ti–P-rich liquid immiscibility in the Duluth Complex, Minnesota. Econ Geol 93:1052–1062
Roedder E (1951) Low-temperature liquid immiscibility in the system K_2O–FeO–Al_2O_3–SiO_2. Am Mineral 36:282–286
Roedder E, Weiblen PW (1971) Petrology of silicate melt inclusions, Apollo 11 and Apollo 12 and terrestrial equivalents. In: Proceedings of Second Lunar Science Conference, Supplement 2. Geochim Cosmochim Acta 1:507–528
Rollinson HR, Windley BF (1980) An Archaean granulite-grade tonalite–trondhjemite–granite suite from Scourie, NW Scotland: geochemistry and origin. Contrib Mineral Petrol 72:265–281
Salisbury S, Boyd J, Rodgers J, McGuire S, Johnson K, Barnes MA, Barnes CG (1999) A method for analyzing extremely iron-rich rock samples (magnetitites) by ICP-AES, and a comparison with other methods. Geol Soc Am, Abstr Program 31:34
Scoates JS, Frost CD, Mitchell JN, Lindsley DH, Frost BR (1996) Residual-liquid origin for a monzonitic intrusion in a mid-Proterozoic anorthosite complex: the Sybille intrusion, Laramie anorthosite complex, Wyoming. Geol Soc Am Bull 108:1357–1371
Srogi L, Lutz TM (1996) The role of residual melt migration in producing compositional diversity in a suite of granitic rocks. Earth Planet Sci Lett 144:563–576
Streckeisen AL (1973) Plutonic rocks: classification and nomenclature recommended by the IUGS subcommission on the systematics of igneous rocks. Geotimes 18:26–30
Taubeneck WH (1964) Cornucopia stock, Wallowa Mountains, northeastern Oregon: field relationships. Geol Soc Am Bull 75:1093–1116
Taubeneck WH (1987) The Wallowa Mountains, northeast Oregon. In: Hill ML (ed) Geological Society of America Centennial Field Guide – Cordilleran Section. Geological Society of America, Boulder, pp 327–332
Taubeneck WH (1995) A closer look at the Bald Mountain batholith, Elkhorn Mountains, and some comparisons with the Wallowa batholith, Wallowa Mountains, northeastern Oregon. US Geol Surv Prof Pap 1438:45–123
Vander Auwera J, Longhi J, Duchesne J-C (1998) A liquid line of descent of the jotunite (hypersthene monzodiorite) suite. J Petrol 39:439–468
Wager RL, Brown GM (1968) Layered igneous rocks. Oliver and Boyd Publishers, London
Watson EB (1976) Two-liquid partition coefficients: experimental data and geochemical implications. Contrib Mineral Petrol 56:119–134
Watson EB, Green TH (1981) Apatite/liquid partition coefficients for the rare earth elements and strontium. Earth Planet Sci Lett 56:405–421
Whitney JA, Hemley JL, Simon FO (1985) The concentration of iron in chloride solutions equilibrated with synthetic granitic compositions: the sulfur-free system. Econ Geol 80:444–460
Wolf MB, London D (1994) Apatite dissolution into peraluminous haplogranitic melts: an experimental study of solubilities and mechanisms. Geochim Cosmochim Acta 58:4127–4145
Wolf MB, Wyllie PJ (1993) Garnet growth during amphibolite anatexis: implications of a garnetiferous restite. J Geol 101: 357–373
Wolf MB, Wyllie PJ (1994) Dehydration-melting of amphibolite at 10 kbar: the effects of temperature and time. Contrib Mineral Petrol 115:369–383
Yurimoto H, Duke EF, Papike JJ, Shearer CK (1990) Are discontinuous chondrite-normalized REE patterns in pegmatitic granite systems the results of monazite fractionation? Geochim Cosmochim Acta 54:2141–2145